THE PHOTOPRODUCTION OF NEUTRAL PIONS FROM HYDROGEN

Thesis by

David Charles Oakley

In Partial Fulfillment of the Requirements

for the Degree of

Doctor of Philosophy

California Institute of Technology

Pasadena, California

1955

ACKNOWLEDGEMENTS

The author wishes to thank Dr. R. L. Walker, who has been most helpful during the course of the experiment and during the author's graduate residence. The many days and evenings that Dr. Walker helped to take data and operate the synchrotron, his many helpful discussions and his inspiration and encouragement cannot be sufficiently acknowledged.

The other members of the synchrotron group have also been most helpful and the author wishes to acknowledge especially the contributions of Dr. R. F. Bacher, Dr. A. V. Tollestrup, Dr. J. C. Keck, Dr. R. V. Langmuir, Dr. M. L. Sands, Dr. J. G. Teasdale, Dr. V. Z. Peterson, chief engineer Bruce Rule, and graduate students J. I. Vette, M. A. Bloch and P. L. Donoho.

The financial support of the U. S. Atomic Energy Commission is gratefully acknowledged.

ABSTRACT

The photoproduction of neutral pions from hydrogen has been studied by counting the recoil protons with a magnetic spectrometer and scintillation counters. The process was studied between photon energies of 260 and 450 MEV and between center of mass pion angles of 70° and 153°. The excitation functions show a resonance type shape with maxima at about 320 MEV. Angular distributions are approximately $\sin^2\theta_\pi^*$ plus a small constant between zero and one third. There is indication of little asymmetry in the angular distributions. The maximum cross section at 90° in the center of mass is 2.56 x 10^{-29} cm^2/steradian for 320 MEV photons. The total cross section divided by the square of the center of mass photon wave length has a maximum at 340 MEV. This quantity drops by about a factor of two at 450 MEV. These results are consistent with magnetic dipole and electric quadrupole absorption leading to a resonant state of the pion-nucleon system of angular momentum $j = 3/2$ and isotopic spin $T = 3/2$.

TABLE OF CONTENTS

I INTRODUCTION

The photoproduction of neutral pions from hydrogen is one of the fundamental experiments to determine the nature of the pion-proton interaction, the key to the understanding of nuclear forces. It is also the least well known of the fundamental experiments, meson-proton scattering and photoproduction of pions from hydrogen. This work reports experimental work done at the California Institute of Technology's synchrotron on the photoproduction of neutral pions from hydrogen.

This reaction has shown (1, 2, 3, 4, 5) a marked difference from the positive pion photoproduction near threshold. The positive production increases about as $(E_\gamma - E_T)^{\frac{1}{2}}$, where E_γ is the gamma ray energy and E_T is the threshold of the reaction. The neutral production increases about as $(E_\gamma - E_T)^{3/2}$ near threshold and at 300 MEV is comparable with the positive production. Weak coupling theory predicts that neutral production should be much smaller than positive production. The energy dependence and nearly isotropic angular distribution of the positive pion photoproduction near threshold indicates a large S state contribution to the cross section. The energy dependence and non-isotropic angular distribution of neutral pion photoproduction near threshold indicates very little S state contribution and the large cross section near 300 MEV is suggestive of a resonance in the P state contribution. Since strong coupling theory predicted a resonance, in pion-proton scattering, of the $P_{3/2}$ state with isotopic spin,

or isospin, T = 3/2, and experiments had shown an indication of this resonance, Brueckner and Case (6) suggested that this state might also be resonant in the photoproduction of neutral pions. Brueckner and Watson (7) used this suggestion to obtain an excitation function.

There have been four methods used to measure the reaction

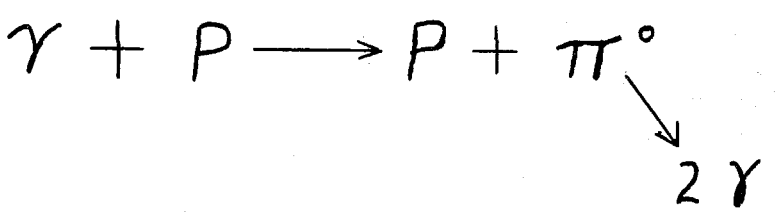

1) detect both gamma rays in coincidence,

2) detect the proton and one gamma ray in coincidence,

3) detect one gamma ray only,

4) detect the proton only.

Steinberger, Panofsky and Steller (1,2) used the first method in their work which pioneered the observation of this phenomenon. This method is not clear cut, but can give a rough idea of the cross section. Method 2) has been used by Silverman and Stearns (3) and later by Walker, Oakley and Tollestrup (4). This method suffers from counting rate difficulties and requires an accurate calibration of the efficiency of the gamma ray counter for detecting at least one of the decay gamma rays from the neutral pion. Method 3) has been used by Cocconi and Silverman (8) for angular distributions and total cross section measurements even though the decay gamma rays are only loosely correlated with the neutral pion.

Method 4) has been used by Goldschmidt-Clermont, Osborne and Scott (5) who counted the recoil protons by photographic plate techniques. This is the method used in this experiment. The proton was identified at a laboratory angle by its momentum and ionization loss. The experiment is capable of attaining good statistics, but requires proof that other processes are not contributing to the flux of protons.

II THEORY

Analysis of the general angular momentum relations of the photon-proton interaction by Feld (9) has produced the following table of angular distributions to be expected for various multipole orders of the absorbed gamma ray and various intermediate states of the system:

γ ray absorbed	Intermediate state	l of mesons	l_j	W (θ_π^*)	π° momentum dependence
Mag. dipole	1/2 +	1	$P_{1/2}$	constant	p^3
Mag. dipole	3/2 +	1	$P_{3/2}$	$2+3\sin^2\theta_\pi^*$	p^3
Elect. dipole	1/2 −	0	$S_{1/2}$	constant	p
Elect. dipole	3/2 −	2	$D_{3/2}$	$2+3\sin^2\theta_\pi^*$	p^5
Elect. quad.	3/2 +	1	$P_{3/2}$	$1+\cos^2\theta_\pi^*$	p^3
Elect. quad.	5/2 +	3	$F_{5/2}$	$1+6\cos^2\theta_\pi^*$ $-5\cos^4\theta_\pi^*$	p^7

(Even parity is +)

However, this table is good for only pure angular momentum and parity state interactions. When the states are not pure, interference can occur between various angular momentum states. One example of the way interference can affect the angular distribution is given by the following equation, derived on the assumptions that only dipole radiation is absorbed and only S and P states are involved:

$$W(\theta_\pi') = |X|^2 + |Y|^2 + |Z|^2 (1 + 3/2 \sin^2\theta_\pi') + 2 \text{ Re } X^*(z-Y)\cos\theta_\pi' - \text{Re } (Y^*Z)\ (3\cos^2\theta_\pi' - 1)$$

where X, Y, Z, are the amplitudes of the $S_{1/2}$, $P_{1/2}$ and $P_{3/2}$ states respectively. Ross (10) has correlated the X, Y, Z terms to the phase shifts observed in meson-proton scattering in an attempt to see what the phase shifts of Fermi and those of Yang imply about the photoproduction cross sections. The curve given in Ross (10) will be compared with the results of this experiment. Notice that the cos θ' term is due to the interference of the S state and the P states. If there is mostly P state contribution to the cross section and the cosine term, that is, the asymmetry in the angular distribution is small, there can be little S state contribution. The apparent lack of this term is part of the reason for the assignment of only P state to the neutral pion photoproduction cross section at energies below 300 MeV.

Once the contributions of the different angular momentum states have been determined for both positive and neutral photoproduction,

one can determine the contributions of different isospin states to this amplitude. For the angular momentum j in terms of the amplitudes of the isospin states T=3/2 and T=1/2 one has:

$$a_j(\pi^0) = \sqrt{2/3}\ a_{j,T\ 3/2} + \sqrt{1/3}\ a_{j,T\ 1/2}$$

$$a_j(\pi^+) = -\sqrt{1/3}\ a_{j,T\ 3/2} + \sqrt{2/3}\ a_{j,T\ 1/2}$$

Since the two j state amplitudes have a different dependence on isospin, the effects of the individual isospin states can be determined. The measurement of the photoproduction of positive pions from hydrogen has been done at the California Institute of Technology's synchrotron and the results will be published soon. Comparison of the results of these two experiments as outlined above should determine the contributions of the individual isospin states.

Bethe and de Hoffman (11) have reviewed the theories and experiments on both pion photoproduction from hydrogen and pion-proton scattering. The theories available for comparison with neutral pion photoproduction are those of Brueckner and Watson (7), Ross (10) and Chew (12). Brueckner and Watson assumed the neutral photoproduction cross section was due to the angular momentum 3/2, isospin 3/2 state from dipole absorption exclusively and found the absolute value of the cross section by fitting their positive cross section to experiment. Ross assumed a coupling constant to fit the photoproduction experiments and used the phase shifts available from meson scattering to find a predicted cross section. Chew used the

cut-off theory for the pion non-relativistic proton interaction and the coupling constant renormalization techniques of Dyson (13) and Ward (14). He then found a coupling constant and a cut-off energy to fit experimental data.

These are the available theories and will be compared with the results of this experiment.

III APPARATUS

The apparatus used in this experiment is shown in figure 1. The photon beam passed through the high pressure hydrogen target. The origin of protons from the photoproduction of neutral pions was defined by the Wolfram slits. Lead bridges 4" above and below a horizontal plane through the beam axis kept stray particles produced in the air from entering the 30 ton, trapezoidal magnet which analyzed the protons by their momentum. The counter house with 4" of lead and 4" of paraffin shielding was placed at the focus conjugate to the Wolfram slits. Inside the counter house were two scintillation counters which differentiated the proton from other particles of the same momentum by the energy loss in the front counter. The beam was monitored by an ionization chamber behind the target.

The 500 MEV bremsstrahlung beam of the California Institute of Technology's synchrotron was collimated by a front collimator and two successive scrapers to eliminate the splatter from the walls of

the front collimator. At the target, the beam was 1 1/2" in diameter.

The hydrogen target consisted of a stainless steel flask of nominal thickness 0.030", 2" in diameter and 17" long, enclosed in a block of styrafoam insulation 6" high by 5" wide, and most of the time further enclosed in a double polyethylene bag of 0.011" total thickness to keep water from condensing on the steel. Attached to the flask was a liquid nitrogen reservoir to cool the gas. Hydrogen was passed through a liquid nitrogen trap each time the target was filled to remove any water vapor. The target was filled to 2000 psi, allowed to cool for about an hour with liquid nitrogen in the reservoir, refilled to 2000 psi and sealed off. Thereafter the liquid nitrogen reservoir was kept filled and the temperature and pressure of the gas were measured periodically to keep track of the density of the hydrogen. The temperature was measured by means of two iron-constantin thermocouples, one at the tip of the target, one close to the liquid nitrogen reservoir. The average of these two readings was compared with the reading of an iron-constantin thermocouple immersed in boiling nitrogen. The temperature of the hydrogen was calculated by using the slope of the iron-constantin calibration table in the Handbook of Chemistry and Physics (15). The density was found by interpolating the data of Johnston et al. (16).

There was considerable background counting rate at some of the settings. This rate was monitored by taking runs with the

hydrogen vented to the atmosphere or pumped below atmospheric pressure by a vacuum pump. Sufficient backgrounds were taken to give approximately the minimum statistical error in the hydrogen-background difference for a given total running time.

The Wolfram slits define the volume of hydrogen used as a source. When looking at protons of momentum greater than that resolvable by the magnetic spectrometer, carbon absorbers were placed at these slits to slow down the protons before they entered the magnet. By putting the absorber at the slits, the Coulomb scattering out of the beam is cancelled by the scattering in. This has been tested by using absorbers of larger atomic number and hence larger mean square scattering angle. These tests show that carbon is a safe absorber to use. The nuclear absorption by the absorbers, the target wall and the air path and nuclear scattering by the absorbers have been corrected for.

The counter house was placed at one of two distances, 208" or 138", called long focus and short focus respectively, from the target. The magnet was placed between the counter house and the target to focus the protons at the counter house. There was a little vertical focussing with the short focus and essentially none with the long focus. The counters were sufficiently high to count all the protons for short focus and an experiment showed a 5.8% correction was needed for those lost with the long focus. The magnet was capable of attaining 15 kilogauss, sufficient to focus protons of 98 or 54 MEV, depending on the focal distance. It had

an aperture, to define the angle and the solid angle, which was varied, when the position of the magnet was changed, in such a way as to keep a sufficiently small range of angles to maintain a reasonable range of photon energies while not sacrificing too much counting rate. The current through the magnet was controlled by a current feedback system except for the 12 1/2° setting when a voltage feedback system was used. When using voltage feedback the current was checked periodically and especially at the beginning and end of the runs.

During the course of the experiment, it was found that the lead bridges used to shield the magnet aperture from stray particles were capable of scattering protons into the aperture that would not have gotten in otherwise. In the later portion of the experiment, the bridges were piled as shown in figure 1. The earlier work had the bridges piled in the dotted position. The effect of the position of these bridges will be discussed in part IX.

The counters used were one of two types. The thick counters were lucite bottles 1" thick, with 1/16" walls, 6" high and 9" long, filled with a liquid scintillator. The thin counters were scintillation plastic furnished by Los Alamos. The front thin counter was 1/4" x 6" x 9" and the back one was 1/2" x 6" x 9". Both sets of counters were surrounded by one mil bright aluminum for a reflector and by a slightly thicker layer of aluminum for light

shielding.

IV ELECTRONICS

The electronics is portrayed in a block diagram in figure 2. The scintillators were viewed by one RCA 5819 photomultiplier tube at each end. The voltages on these tubes were adjusted to give the same pulse height in each of the two looking at the same scintillator. Their outputs were then connected in parallel.

The outputs of the counters were first preamplified near the counter house and then the pulses were led to the counting area where they were amplified by model 522A amplifiers which had a rise time of 0.07 microsecond and a fall time of 0.10 microsecond. The first amplifier had an output going to the coincidence circuit and one to the gating circuit. The second amplifier had an output to the coincidence circuit and one to a fast discriminator which provided a monitor of the singles counting rate. The coincidence circuit had an output which provided a signal for each pulse from the first counter that exceeded the bias required by the coincidence circuit. This was led to another fast discriminator to monitor the singles counting rate in the first counter.

When looking at protons with sufficient energy to pass through the first counter, it was possible to require a coincidence between the first and second counter. One output of the coincidence circuit then was used to gate the signal from the first counter. The

coincidence circuit also provided signals to monitor the number of coincidence counts and signals to monitor the accidental counting rate by counting the number of times a pulse from the first counter was in coincidence with a delayed pulse from the second counter. The delay was 0.8 microsecond, sufficiently short to sample corresponding singles rates in the two counters.

When coincidences were required, the gating circuit passed the pulse from the first amplifier when a gating signal was received from the coincidence circuit. When the protons could not all get through the first scintillator, the gating circuit was set to merely pass all the signals from the first amplifier.

The gated signal then went to a stack of 8 discriminators which each gave the number of counts above its bias setting. The biases were set at equal intervals. By subtracting adjacent integral counting rates a differential bias spectrum was obtained for each run. In most cases the proton peak was well separated from the mesons in this differential spectrum. In some cases, however, particularly when no coincidence was required, it was necessary to subtract corresponding background runs to get clear separation of the peaks.

The total energy in the bremsstrahlung beam was monitored by a Cornell type ionization chamber with the output integrated by an ion current integrator. This chamber has 1" thick copper walls. This thickness is very close to the peak of the shower curve for a

wide range of energies. The output is nearly proportional to the total energy, independent of the maximum energy of the beam. This ion chamber and current integrator have been calibrated by a pair spectrometer and also by the shower method of Blocker, Kenney and Panofsky (17). Comparison of these calibrations will be discussed under errors in part IX. Standard runs were 50 or 100 Beam Integrator pulses, known as BIPs. The temperature of the ionization chamber and the atmospheric pressure were taken periodically to take account of the ion-chamber changes with these variables.

The magnetic field of the synchrotron during the dumping of the beam into the target was also read periodically. This was used for a first order correction to the number of photons for small changes in the maximum energy of the bremsstrahlung beam.

V EXPERIMENTAL DETAILS

Due to the size of the magnet and counter house and the need for restacking the lead bridges after each magnet move, it was convenient to set the spectrometer in place and then make runs with different currents and absorbers, getting all runs, including backgrounds before moving the magnet again. This procedure gives excitation functions for constant laboratory angles. Angular distributions at constant photon energy are obtained from these by reading the excitation curves at the desired energy and plotting these values at the center of mass angle appropriate for the photon energy and

laboratory angle involved.

The thick counters were used for one setting of the magnet and thin counters for the rest of the work. The nominal angles, focal lengths and counters used were:

12 1/2 degrees	long focus	thick counters
19 1/2 degrees	long focus	thin counters
29 degrees	short focus	thin counters
40 1/2 degrees	short focus	thin counters
50 1/4 degrees	short focus	thin counters

When counting only the recoil proton from the reaction one is not certain that the neutral pion was produced. The proton Compton effect from photons of a particular energy is capable of giving protons of the same energy as neutral pion production from photons of higher energy. Hence if one looks for protons from neutral pion photoproduction by photons above the bremsstrahlung limit one can determine the effect of the Compton effect on the measurement. This has been done at two settings by putting more absorber at the slits. It was also done at the 40 1/2 degree setting by reducing the synchrotron energy in steps, while leaving the magnetic spectrometer at a particular setting. The results of these tests are discussed in part IX.

The field of the magnetic spectrometer was calibrated as a function of current by a proton resonance apparatus. During the

course of this calibration it was found that the hysteresis in the magnet was about 1% of the field. This was discovered at a late date in the experiment and cannot be corrected.

VI DATA REDUCTION

Having found the counting rate it is necessary to convert it into a cross section in the center of mass system by the following formula:

$$C = \frac{d\sigma}{d\Omega'} \frac{d\Omega'}{d\Omega} \Delta\Omega \; N(H_2) \; \eta(k_i) \Delta k_i \; a$$

C is the counting rate per BIP corrected for background. (Accidentals were always negligible.)

$\frac{d\sigma}{d\Omega'}$ is the differential cross section in the center of mass system.

$\frac{d\Omega'}{d\Omega}$ is the ratio of center of mass to laboratory solid angle at the given laboratory angle and energy.

$\Delta\Omega$ is the laboratory solid angle.

$N(H_2)$ is the number of hydrogen atoms per square centimeter normal to the photon beam defined by the Wolfram slits.

$\eta(k_i)$ is the number of photons per BIP of energy k_i per MEV.

Δk_i is the range of photon energies corresponding to the range of proton energies defined by the counters.

a is a correction for absorption and scattering in the target, absorbers, air path and scintillators.

First order corrections were made to take account of the variation in the ion chamber response with temperature and atmospheric pressure and to take account of the variation in $\eta(k_i)$ with maximum energy of the bremsstrahlung. Since these readings were taken at the same time as the density readings, their effects were most conveniently lumped together into the density. Each hydrogen run was given an effective density interpolated between readings.

$$\eta_o(k_i) = \eta(k_i) \frac{P}{760} \frac{273}{T} \frac{B_o}{B}$$

$$\bar{\rho} = \rho \Big/ \left(\frac{P}{760} \frac{273}{T} \frac{B_o}{B}\right)$$

$\eta_o(k_i)$ is the number of photons per BIP per MEV for the ion chamber at 760 mm Hg pressure and at 273° Kelvin with a 500 MEV bremsstrahlung. This is now put in the previous formula in place of $\eta(k_i)$

$\bar{\rho}$ is the effective density and is now used in calculating $N(H_2)$.

P is the atmospheric pressure in mm of Hg.

T is the Kelvin temperature of the ion chamber.

B_o is the magnetic field to give 500 MEV bremsstrahlung.

B is the measured peak magnetic field.

The fringe field of the magnetic spectrometer was analyzed by Dr. R. L. Walker, who found an effective edge of the magnet. He has also found the radii of curvature for the two focal distances. Knowing the radius of curvature and the field determines the momentum resolved, but the range of momenta is determined by the width of the counters. A 1:4 scale drawing of the spectrometer was used to find the range of momenta accepted by the counters. This is a function of the position of the beam as it enters the magnet and varies by 30% over the aperture used, as shown in figure 3. An average value was found by weighting the range of momenta by the solid angle of a small element of the aperture and integrating numerically over the aperture used at each setting, for both no coincidence and coincidence counting since the different physical position of the front and back counters gave different ranges of momenta. Also in the process of finding the average range of momenta, the average angle was found by weighting each angle by the solid angle and the range of momenta associated with a small element of aperture. This is the angle used in the calculations, but it did not vary from the nominal angle by more than a few minutes and is a negligible correction.

The correct relativistic formulas were used to calculate the

kinetics of each individual angle and momentum observed. First, knowing the momentum of the proton passed by the magnetic spectrometer, and the range of momenta accepted, one obtains the energy and range of energies measured by the magnetic spectrometer:

$$T^* = \sqrt{(P^*)^2 + M^2} - M$$

$$\Delta T^* = \frac{(P^*)^2}{T^* + M} \frac{\Delta P^*}{P^*}$$

Starred quantities are measured. T^* is proton kinetic energy. P^* is the measured proton momentum. M is the proton mass (938.2 MEV.)

This energy and range of energies must be converted to ranges since in all cases the target wall thickness is too large to use an approximation. Since carbon absorbers were used when necessary, the thickness of the components of the target wall and the air between the target and the magnetic spectrometer were converted to equivalent grams per square centimeter of carbon by means of Bakker and Segre's results (18), while assuming a proton energy of 30 MEV. The energy of the proton makes a negligible change in the conversion to carbon equivalent, but is most sensitive for low energies near 30 MEV, so this energy was assumed for all runs even though some protons passed through the target wall with 200 MEV energy. Since the target was cylindrical, the thicknesses of the steel, styrafoam and hydrogen were variable depending on the distance off the

horizontal plane through the axis. The thicknesses of carbon equivalent to the steel, polyethylene, styrafoam and hydrogen were weighted by the amount of hydrogen available to the reaction, added together and averaged to find an average thickness. This average thickness was divided by the sine of the angle of observation and added to the equivalent thickness of the air and any absorbers that were in the proton beam to get the total absorber the proton was forced to pass through.

The range of energies accepted by the spectrometer is greater than the range of energies that these same protons had when they were inside the target due to the fact that those with less energy inside the target would lose more energy in getting through the absorber than those with more energy inside the target. The energy and range of energies inside the target is found by these relations:

$$R(T) = \overline{\Delta R^*}_{WALL} + \Delta R^*_{ABSORBER} + R^*(T^*)$$

$$\Delta T = \frac{dT/dx}{dT^*/dx} \Delta T^*$$

Starred terms refer to measured quantities and unstarred refer to values inside the target. The relations between ranges, energies and specific ionization were taken from Aaron (19).

Knowing the energy and range of energies the protons had when inside the target, the photon energy and range of energies was found

by the following:

$$k_i = \frac{TM + m_\pi^2/2}{P\cos\theta_p - T}$$

$$\Delta k_i = \Delta T \left(\frac{dk_i}{dT}\right)_{\theta_p} = \Delta T \frac{M + k_i\left(1 - \frac{E}{P}\cos\theta_p\right)}{P\cos\theta_p - T}$$

k_i is the incident photon energy.

θ_p is the proton laboratory angle.

m_π is the neutral pion mass (135.1 MEV).

The ratio of center of mass solid angle to laboratory solid angle comes from the formula (20).

$$\frac{d\Omega'}{d\Omega} = \frac{\left(1 - \frac{\beta_{cm}}{\beta_p}\cos\theta_p\right)\left[1 + \left(\frac{\beta_{cm}}{\beta_p}\right)^2 - 2\frac{\beta_{cm}}{\beta_p}\cos\theta_p - \beta_{cm}^2\sin^2\theta_p\right]^{1/2}}{1 - \beta_{cm}^2}$$

$$\beta_{cm} = \frac{k_i}{k_i + M} \qquad \beta_p = \frac{\sqrt{T^2 + 2TM}}{T + M}$$

$\eta(k_i)$, the number of photons per MEV of the bremsstrahlung spectrum was obtained from the theoretical spectrum with a correction for the differences in synchrotron energy during the beam dump cycle, which has been checked at the synchrotron laboratory by a pair spectrometer, the ion chamber calibration, 4.259×10^{18} MEV/coulomb

and the current integrator calibration, 2.35×10^{-7} coulomb/BIP for integrator M-1, scale #3. These last two calibrations are the source of the biggest uncertainty in the absolute cross section and will be discussed in part IX.

a is the correction for nuclear absorption and nuclear and Coulomb multiple scattering of the protons by the target walls, absorbers, air path and scintillators. The absorption cross section was calculated by the theory of Fernbach, Serber and Taylor (21) with the energy dependent parameters determined by Taylor (22). The absorption cross section was plotted as a function of residual range and was integrated for each setting from the residual range of the proton upon entering the final scintillator to the residual range the proton had at the center of the target. The absorption correction was generally a few percent but ranged as high as 35% for those settings requiring the most absorber. Nuclear and Coulomb multiple scattering from the air path were neglected and the scattering out by the target walls was assumed to be compensated by the scattering in. Nuclear scattering was neglected in the first scintillator. Coulomb multiple scattering in the first scintillator was calculated to be less than 1% correction for thick counters, assuming uniform distribution of the protons across the scintillators. For the long focus arrangement a measurement was made to test the amount of vertical focussing and the scattering

in the first counter by reducing the height of the magnet aperture from 3" to 2". The 2" aperture counted 5.8 ± 2.9% more than the 3" aperture when corrected to equal solid angle. This correction was used for the long focus arrangement, but no correction was used for short focus since thinner counters were used and there was some vertical focussing in those arrangements, both effects decreasing the correction. The correction for nuclear scattering by the carbon absorbers was calculated from the geometry of the setting and the nuclear scattering cross section as determined by subtracting the nuclear absorption cross sections mentioned above from the total neutron cross sections listed in Rossi (23). The Coulomb multiple scattering had such a small mean square scattering angle, that its effects were neglected. It was checked by using absorbers of different atomic number and will be discussed in part IX.

VII EXCITATION FUNCTIONS

The excitation functions are shown in figures 4 through 8, for proton laboratory angles 12 1/2, 19 1/2, 29, 40 1/2 and 50 1/4 degrees respectively. The cross sections are in the center of mass system while the photon energies are in the laboratory system. Those points that have two errors have been obtained from the first set of experiments in which the protons were found to scatter from the protective lead bridges. A correction factor

was determined from the ratio of the second to the first set cross sections. The points with the double errors were obtained from the first set by multiplying by this factor. The smaller errors are the statistical errors discussed below, while the larger errors include the error in the correction factor. The entire 12 1/2° experiment, figure 4, is from the first set, with no correction factor. Part IX will discuss the reasons for this procedure. The points with only one error are computed from the second set of experiments. The triangles denote points that could not make use of the coincidence technique of counting the protons, while the circles denote the use of coincidence between the two counters to trigger the gating circuit.

The energy resolution functions are shown at the bottom of each figure for various representative settings. These settings were chosen so that the shapes of the functions vary smoothly between the figures shown. These resolution functions include the effects of the angular resolution as well as the momentum resolution. The unusual resolution functions in figure 4, 12 1/2°, are due to the target wall. The lower energy peak came from those protons which came through the cap of the target, losing much less energy than those protons that came through the side wall which provides the higher energy peak.

The errors on the points are standard deviations and are composed of statistical errors. The dotted curves are estimated

standard deviations of the systematic errors with the exception of two systematic errors which can be corrected if better values are obtained, the ion chamber-current integrator calibration and the ratio of the range of momenta to the central momentum resolved, $\Delta p^*/p^*$. A table of errors will be included in part IX.

VIII ANGULAR DISTRIBUTIONS

The pion center of mass angles can be found from the velocities of the proton and the center of mass and the angle of the proton in the laboratory system by:

$$\tan \theta_\pi' = \frac{-\sqrt{1-\beta_{CM}^2}\,\sin\theta_p}{\frac{-\beta_{CM}}{\beta_p} + \cos\theta_p}$$

By this transformation one can take values of the cross section for a particular photon energy from each laboratory angle and plot an angular distribution in the center of mass system. This has been done and is shown in figure 9 with a logarithmic ordinate and tabulated in table I. The center of mass angular resolutions are shown at the bottom of figure 9 with a linear ordinate.

The solid curves are a least squares fit to a form:

$$A + B\cos\theta_\pi' + C\cos^2\theta_\pi'$$

The values of these coefficients as a function of photon laboratory energy are shown in figure 10. In figure 9, the dotted curve for 270 MEV is obtained from the intersection of the three curves for A, B and C with 270 MEV in figure 10, showing that the curves for these parameters are not inconsistent with the three points that were measured at this energy.

The angular distribution is also fitted to a form:

$$A + C \cos^2 \theta'_\pi$$

in figure 11. The curves are the central curves for A and C from figure 10.

Since the data extend only to 70° at most, the odd powers of $\cos\theta'_\pi$ could not be well determined in an infinite power series of $\cos\theta'_\pi$. However, by restriction of the power series to at most terms of second order, the first power determines the slope of the angular distribution near 90°. If B were made as large as either A or C, one would not be able to fit the data satisfactorily.

Assuming the coefficients of the power series $A+B\cos\theta'_\pi + C\cos^2\theta'_\pi$ as was obtained by the least squares fit, the total cross section is:

k_i	(Lab MEV)	295	320	360	400	450
σ	(10^{-29}cm^2)	20.5	21.8	19.1	13.1	7.8

This cross section divided by the square of the center of mass photon wave length is plotted in figure 12.

IX ERRORS

The statistical errors assigned to the points in the excitation functions include:

Counting statistics and estimate of error in separating the proton peak from the pion peak.

Error due to part of the beam dumping before the gating circuit opened the counters = +0% -1%.

Uncertainty in resetting the magnetic analyzer field = ± 1%.

Error in reading target thermocouple voltages = ± 3/4%.

Error in reading target pressure = ± 1/2%.

The systematic errors of the experiment are of two types, those that depend on the proton energy and those that do not. Those depending on the proton energy are:

Target wall thickness = ± 5% of thickness.

Absorber thickness = ±1% of thickness.

Absorber scattering and absorption = ± 10% of total correction.

Slit penetration = ± 2% to nothing.

Proton angle setting = ±1/4° (at 12 1/2° = ±1°).

Those not depending on the proton energy are:

Temperature of target gas = ±2°K = ±2%.

Pressure of target gas due to reading gauge rather than absolute pressure = +0% -1/2%.

Ion chamber sensitivity stability = ±0.1%.

Current integrator stability = ± 1.5%.

Error in vertical focussing correction,

(short focus) = ± 0%,

(long focus) = ± 3%.

The mean square scattering angle for Coulomb scattering from a moderately thick piece of carbon in the proton beam is 2.2°, for pieces of aluminum, copper and lead of about the same energy loss it is 3.4°, 5.1° and 9.0° respectively. These materials were tested as absorber materials and the results are shown in figure 13. By assuming that the difference in the cross sections from the aluminum, copper and lead points and carbon curve is due to protons that were scattered beyond a critical angle, the critical angle can be obtained and then the amount of the cross section lost by using carbon absorbers can be found. In none of the five cases is this loss greater than 0.1%. This effect has been ignored and no error is assigned to it.

The effects of nuclear absorption and nuclear scattering were analyzed by the theory of Fernbach, Serber and Taylor (21) with the energy dependent parameters determined by Taylor (22). Their agreement with neutron cross sections seems to be very good.

On the assumption of charge independence, the nuclear effects of protons on carbon should be well known. The error assigned to this calculation was ± 10% of the correction, and seems to be a conservative estimate considering the agreement Taylor obtained with experiment.

A set of runs was made with the lead bridges shown in figure 1 in the position of the dotted lines. These runs did not show very good internal consistency and further runs showed that by moving the bridges to the position shown in figure 1 the cross sections changed as shown in figures 14 through 17. With the bridges moved back from the beam, a proton would have to scatter through a much larger angle to get into the magnet aperture than with them very close to the beam. Backgrounds were much higher when no bridges were used, so the bridges were moved away from the beam and it is assumed that a negligible fraction of the protons analyzed come from scattering from the bridges. At the 12 1/2° setting the bridges were made of 2" thick lead bricks alternated with 2" air spaces on one side extending from the target to the magnet and a solid bridge of bricks on the other side extending only about 2/3 of the distance from the magnet to the target. The other settings used solid bridges on both sides extending all the way from the target to the magnet. The 12 1/2° bridges were fairly close to the proton beam, but due to the difference in the method of stacking them, it would not be correct

to use the correction factors determined for the other settings. This setting is reported as observed, but the correction factors determined from the other settings are included in the estimate of the possible range of the excitation curve as shown dotted in figure 4.

The Coulomb multiple scattering of the front counter, was calculated to be less than a one percent correction for the thick counters used at 12 1/2°. A 2" aperture at the magnet gave 5.8 ± 2.9% more counts per steradian than a 3" aperture. This measurement finds the number of protons that do not strike the front counter or are scattered in it sufficiently to miss the second counter in the long focus arrangement. The error is included in the systematic errors described above. The thinner counters used for all angles other than 12 1/2° would have even less correction if protons were uniformly distributed over the front counter. The short focus configuration had some vertical focussing and did not uniformly distribute protons out to the edge of the front counter. Therefore no correction was made for this effect for short focus runs and no error is assigned.

Coulomb and nuclear scattering from the air path from the target was ignored since so little material was involved. No error is assigned.

Measurements of the possible contribution of the proton Compton effect:

$$\gamma + P \longrightarrow P' + \gamma'$$

are shown in figures 18 and 19. Figure 18 depicts a set of runs with the magnetic spectrometer set at 40 1/2°, resolving protons of 70.1 MEV as shown in a small portion of the kinetics curves of proton energy versus proton angle for various photon energies with both processes indicated. The peak energy of the bremsstrahlung was reduced from 500 to 400, 350, 325 and 300 MEV. The counting rates, corrected for variations in hydrogen density in the target, are plotted versus the synchrotron peak energy. Figure 19 shows runs at two angles with carbon absorbers of sufficient thickness to resolve protons coming from photons, assuming neutral pion photoproduction of energy at or above the synchrotron peak energy of 500 MEV, or assuming proton Compton effect, energies about 40 MEV less. The combined conclusions would be that the Compton cross section makes up less than 5×10^{-31} cm^2/steradian of the neutral pion photoproduction cross sections.

One of the correctable errors is the ratio of the range of momenta to the central momentum resolved by the magnetic spectrometer, $\Delta P^2/P^2$. The determination used was a graphical construction, assuming a particular effective field to correct for the fringe field effects. If a more satisfactory determination

were made, each excitation function could be corrected by multiplying by the ratio of old to new values since this function enters into the calculation of the cross section inversely. An estimate of the error involved in this calculation would be $\pm$ 2%.

The other correctable error is the calibration of the ion chamber and the associated current integrator. Two calibrations of the ion chamber have been made at the synchrotron. One was a pair spectrometer calibration by Cooper (24). This method calibrates the ion chamber and integrator combination, giving the number of MEV/BIP. The shower curve method of Blocker, Kenney and Panofsky was performed by Keck (25). This method determines the number of MEV/coulomb directly, but requiring an accurate knowledge of the number of electron volts per ion pair in air. To compare these two calibrations requires a measurement of the charge sensitivity of the integrator. Cooper did this by measuring the time required to collect a BIP with a known current input. There is some question about the accuracy with which this current was known, involving the voltage sensitivity of a 940 megohm resistance.

Measurement of the charge sensitivity has given values ranging from 2.35 to 2.45 x 10^{-7}coulombs/BIP. This gives a total range of 4% variation which might be due to variations in the integrator or current limiting resistor. Another calibrator

later became available, Model 10, which charges a precision air capacitor with potentiometer measured voltage and then discharges into the integrator. These two calibrators were tried one after the other. The current source gave a value 2.43×10^{-7} coulombs/BIP while the charge source gave a value 2.27×10^{-7} coulombs/BIP, a difference of 7%. The quoted voltage coefficient of this resistor could make up this difference and it is felt that the charge source is the more reliable method of calibration. However, 2.27×10^{-7} coulombs/BIP would increase the discrepancy between the Cooper and Keck calibrations of the ion chamber from 8% to 12%, well outside the error of 5%. Measurements with the Model 10 calibrator have shown a 4% total range of values over a period of a month, as was observed with the current source. The calibrations used in this experiment were: ion chamber calibration 4.259×10^{18} MEV/coulomb and current integrator calibration 2.35×10^{-7} coulomb/BIP. The ion chamber calibration is an average of the two calibrations and the current integrator calibration is also an average of its calibrations. The error in this effect will be assigned at ± 6%, with an additional ± 1 1/2% for stability which has been tabulated above in the systematic errors.

X COMPARISON WITH OTHER WORKS

The results of Goldschmidt-Clermont, Osborne and Scott (5)

of Massachusetts Institute of Technology have been normalized to fit smoothly onto the A pictured in figure 10. The curve of A below 295 MEV was drawn so that it would be proportional to $(E_\gamma - E_p)^{3/2}$, the energy dependence to be expected from a P state interaction (9). The normalized M. I. T. points fit reasonably to this curve. Also on figure 10 are the experimental points of Silverman and Stearns (3) of Cornell who determined an absolute cross section. These points would not fit smoothly onto A from this experiment. Walker, Oakley and Tollestrup (4) also used the method of Silverman and Stearns. They got a slightly higher value than Cornell, but closer to that than to the A of this experiment. Walker et al. now feel (26) that the preliminary experiment reported in (4) used an unsuitable estimate for the gamma ray counter efficiency. Therefore their work is not compared. They have preliminary results, using an improved gamma ray counter, which are in fair agreement with the angular distributions found in this experiment. Even with good gamma ray counters the calculation of the probability of detecting at least one of the decay gamma rays from the neutral pion is difficult to do accurately. It may be that Silverman and Stearns had the same difficulty as Walker et al. They did quote an error of ± 30%, but this experiment gives A about 80% above their value.

Brueckner and Watson (7) predicted an angular distribution

of $5 - 3\cos^2\theta'_\pi$ if there were a pure $j = 3/2$, $T = 3/2$ state interaction from dipole absorption. The angular distribution is not like this prediction and indicates that electric quadrupole absorption is probably important. If there were much S state contribution, B, the coefficient of $\cos\theta'_\pi$ in the angular distribution which arises from interference between S and P states, would be larger than is found in figure 10.

Comparison with Chew's cut-off meson theory (12) is shown by figure 20. This theory predicts an angular distribution:

$$\frac{d\sigma}{d\Omega'} = \frac{4e^2f^2}{\mu^2}\,v\left\{|M_1 - E_2|^2\cos^2\theta'_\pi + \left[2|M_1|^2 + \tfrac{1}{2}|M_1 + E_2|^2\right]\sin^2\theta'_\pi\right\}$$

$$M_1 = X\,\frac{v}{k^2}\,e^{i\delta_{33}}\sin\delta_{33}$$

$$E_2 = Y\,\frac{v}{k^2}\,e^{i\delta_{33}}\sin\delta_{33}$$

f^2 is Chew's renormalized coupling constant = 0.055,

μ is the pion mass,

v is the pion velocity,

ν is the photon momentum,

k is the pion momentum,

δ_{33} is the $j = 3/2$, $T = 3/2$ phase shift from pion-nucleon scattering,

M_1 is the magnetic dipole absorption matrix element,

E_2 is the electric quadrupole absorption matrix element. To fit the values of A and B with Chew's calculated phase shifts (27) requires X = .79 and Y = .45 and with Bethe's phase shifts (11,28), X = .81 and Y = .40. The pion-nucleon phase shifts have not been analyzed to high enough energy to fit the 400 and the 450 MEV plints, so phase shifts were chosen for these points for the two sets. The angles used for the points in figure 20 are given in table II. The fit is reasonably good with either of these sets of phase shifts although Bethe's fall off a little too rapidly in the lower energies. It should be pointed out that Chew's theory is in a preliminary form only.

Ross (10) gives an equation:

$$\frac{d\sigma}{d\Omega'}(90^\circ) \sim \sin^2(\delta_{33} + \alpha)$$

with which phase shifts can be determined. These are given in table II. These are considerably different than either Chew's or Bethe's. This is because he does not have the dependence on meson momentum that Chew does. He also shows the two types of photoproduction cross sections to be expected if the phase shift passes through 90° or not. The coefficient A, the 90° cross section in the center of mass, matches Ross' curve for the phase shift passing through 90° but is higher at both higher and lower energies.

XI CONCLUSIONS

The neutral pion photoproduction is consistent with a phase shift of the $j = 3/2$, $T = 3/2$ pion nucleon interaction that passes through 90°. The angular distribution, while not as complete as is desirable to determine asymmetry, shows little indication of a $\cos \theta_{\pi}^{*}$ term and thus little indication of S wave contribution to the cross section. C, the coefficient of $\cos^{2}\theta_{\pi}^{*}$ is 75% to 100% of A, the constant, indicating that electric quadrupole absorption is probably important.

The data are now available for the neutral pion photoproduction. More detailed analysis must wait for the results of the positive pion photoproduction experiments, soon to be published from this laboratory. Then the phenomenology of pion photoproduction should be fairly well understood. However, due to the limitations of the experimental apparatus, this experiment was limited to θ_{π}^{*} greater than 70° and to photon energies greater than 260 MEV. There is still a great deal of information that should be obtained at smaller angles and lower energies.

REFERENCES

(1) J. Steinberger, W. K. H. Panofsky and J. S. Steller
Phys, Rev. 78 802 (1950)

(2) W. K. H. Panofsky, J. N. Steinberger and J. Steller
Phys. Rev. 86 180 (1952)

(3) A. Silverman and M. Stearns
Phys. Rev. 88 1225 (1952)

(4) R. L. Walker, D. C. Oakley and A. V. Tollestrup
Phys. Rev. 89 1301 L (1953)

(5) Y. Goldschmidt-Clermont, L. S. Osborne and M. S. Scott
Phys. Rev. 89 329 L (1953)

(6) K. A. Brueckner and K. M. Case
Phys. Rev. 83 1141 (1951)

(7) K. A. Brueckner and K. M. Watson
Phys. Rev. 86 923 (1952)

(8) G. Cocconi and A. Silverman
Phys. Rev. 88 1230 (1952)

(9) Bernard T. Feld
Phys. Rev. 89 330 L (1953)

(10) Marc Ross

Phys. Rev. 94 454 (1954)

(11) H. Bethe and F. de Hoffman

"Mesons and Fields", Vol. II, Row, Peterson and Company (to be published)

(12) G. F. Chew (Preprint of paper)

(13) F. J. Dyson

Phys. Rev. 75 1736 (1949)

(14) J. C. Ward

Proc. Phys. Soc. Lond. 64A 54 (1951)

(15) C. D. Hodgman,

Editor, "Handbook of Chemistry and Physics" (1947) 30th Edition, 1979

(16) H. L. Johnston, I. I. Bezman, T. Rubin, C. A. Swanson, W. Corak and E. B. Rifkin, "Low Temperature, High Pressure Data of State for Hydrogen and for Deuterium between 64° and 300° K.", AEC MDDC-850

(17) W. Blocker, R. W. Kenney and W. K. H. Panofsky

Phys. Rev. 79 419 (1950)

(18) C. J. Bakker and E. Segre

Phys. Rev. 81 489 (1951)

(19) W. A. Aaron, University of California Radiation Laboratory Report #1325 (1951)

(20) Martin Wiener, National Bureau of Standards Circular 515 (1951)

(21) S. Fernbach, R. Serber and T. B. Taylor

Phys. Rev. 75 1352 (1949)

(22) T. B. Taylor

Phys. Rev. 92 831 L (1953)

(23) Bruno Rossi

"High Energy Particles" (1952) 344

(24) D. H. Cooper, Thesis, California Institute of Technology, (1955)

(25) J. C. Keck (private communication, see also synchrotron laboratory notebook #63)

(26) R. L. Walker, D. C. Oakley and A. V. Tollestrup

(private communication)

(27) Geoffrey F. Chew

Phys. Rev. 95 285 L (1954)

(28) H. A. Bethe and F. de Hoffman

(preprint of letter to appear in the Physical Review)

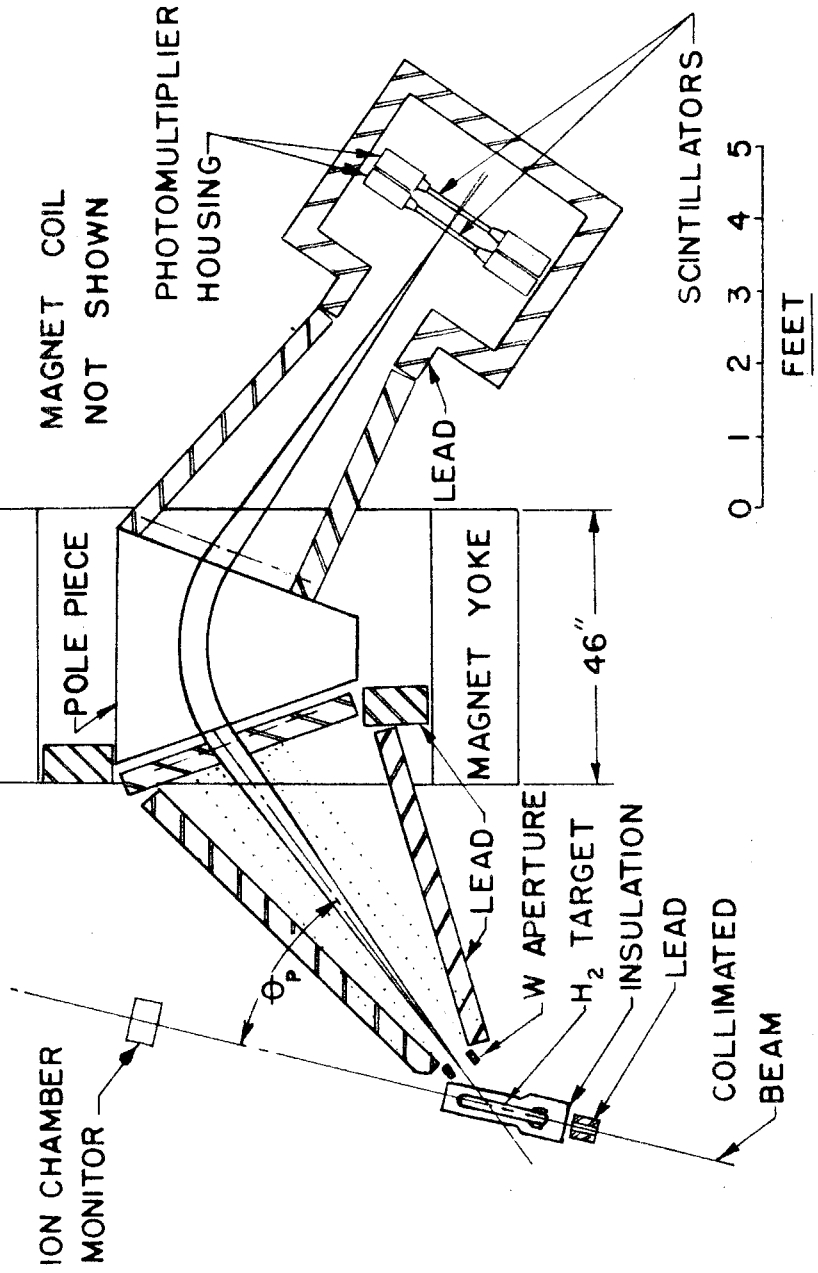
ION CHAMBER MONITOR
COLLIMATED BEAM
LEAD
INSULATION
H_2 TARGET
W APERTURE
LEAD
MAGNET YOKE
POLE PIECE
46"
LEAD
PHOTOMULTIPLIER HOUSING
MAGNET COIL NOT SHOWN
SCINTILLATORS
0 1 2 3 4 5
FEET

FIG. 1

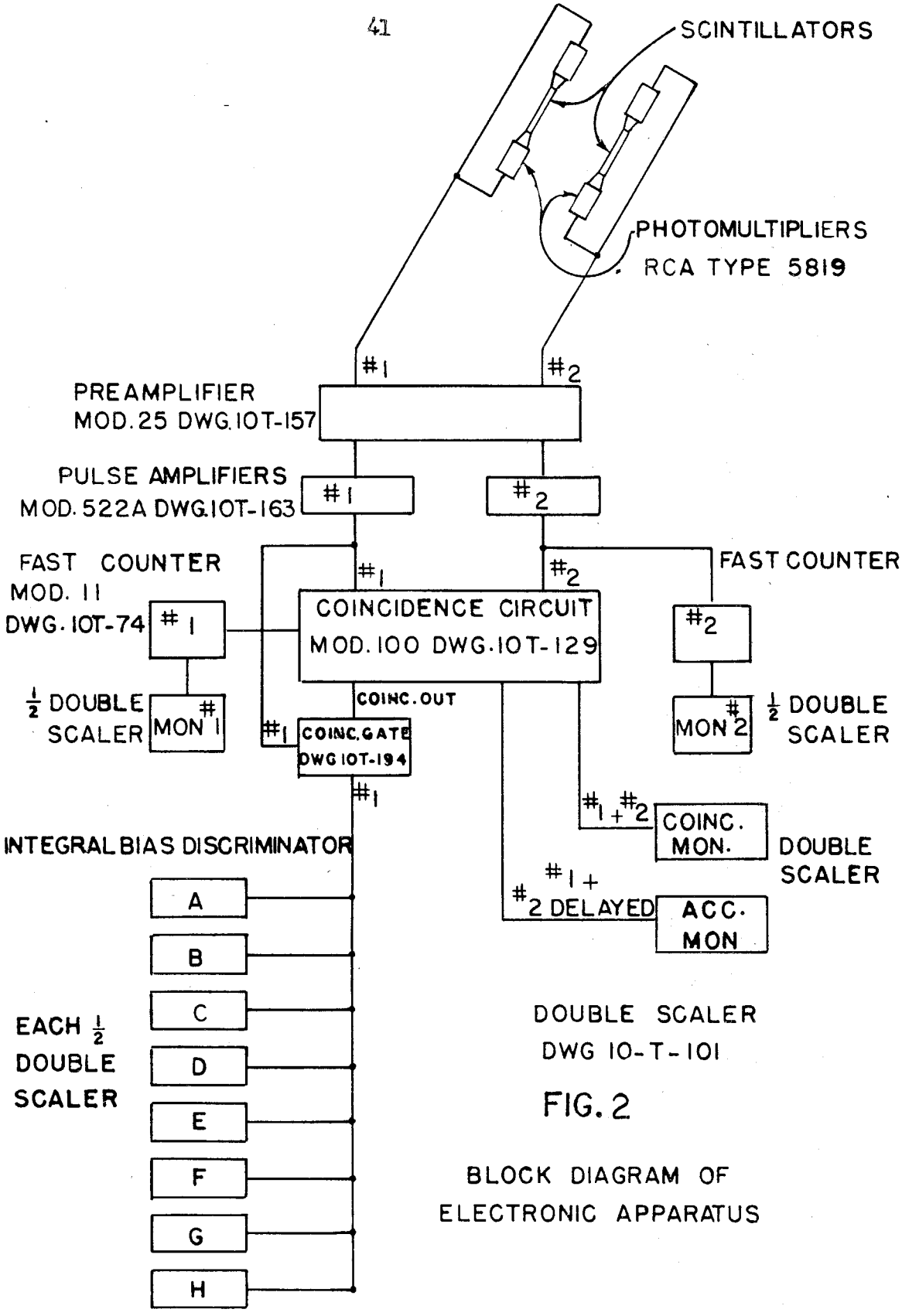

FIG. 2

BLOCK DIAGRAM OF
ELECTRONIC APPARATUS

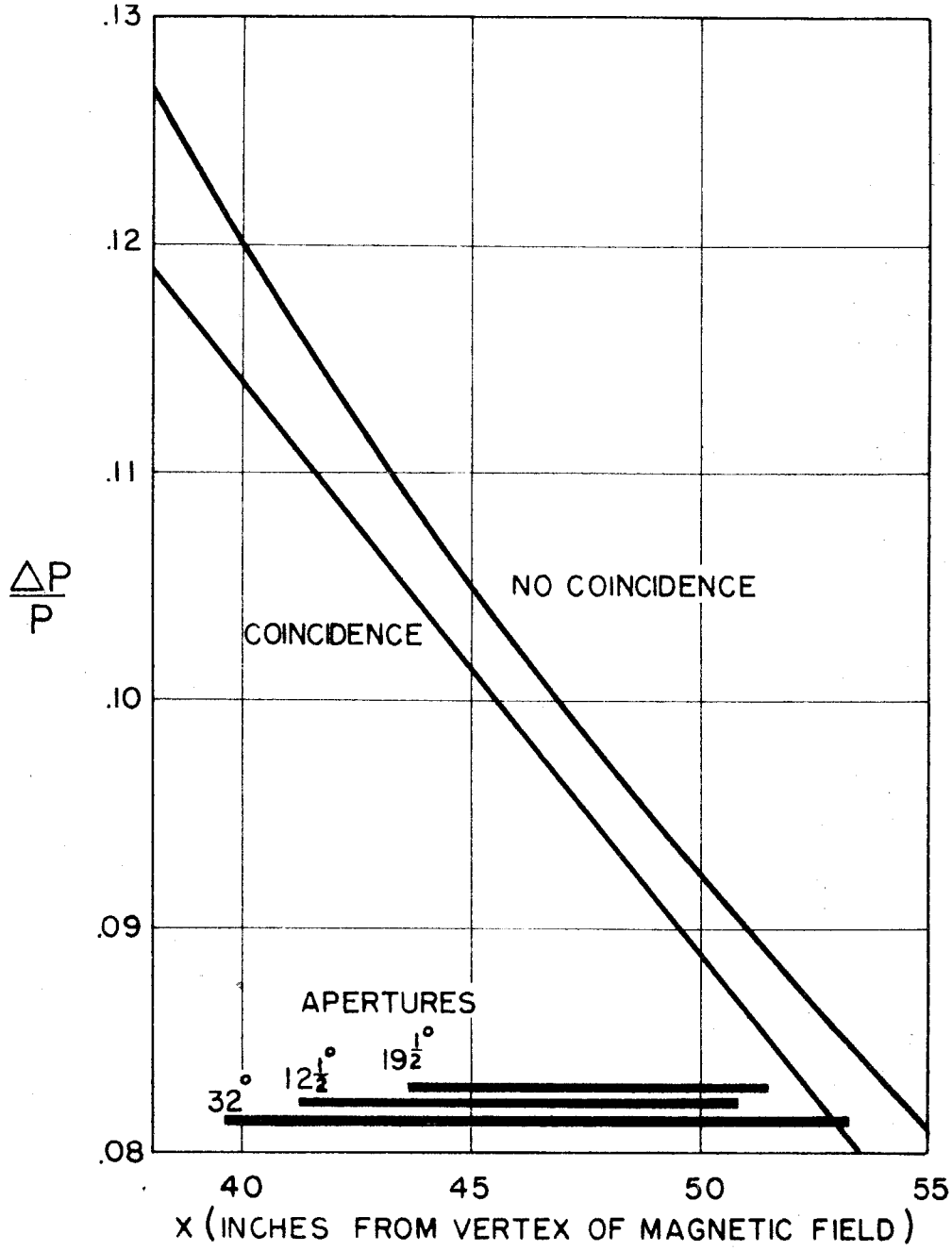

FIG. 3

RELATIVE RANGE OF MOMENTA ACCEPTED
BY COUNTERS WITH LONG FOCUS

$$\gamma + P \longrightarrow P + \pi^{\circ}$$

Center of mass differential cross section

for proton laboratory angle, θ_p = 12 1/2°

California Institute of Technology
July 31, 1954

FIG. 4

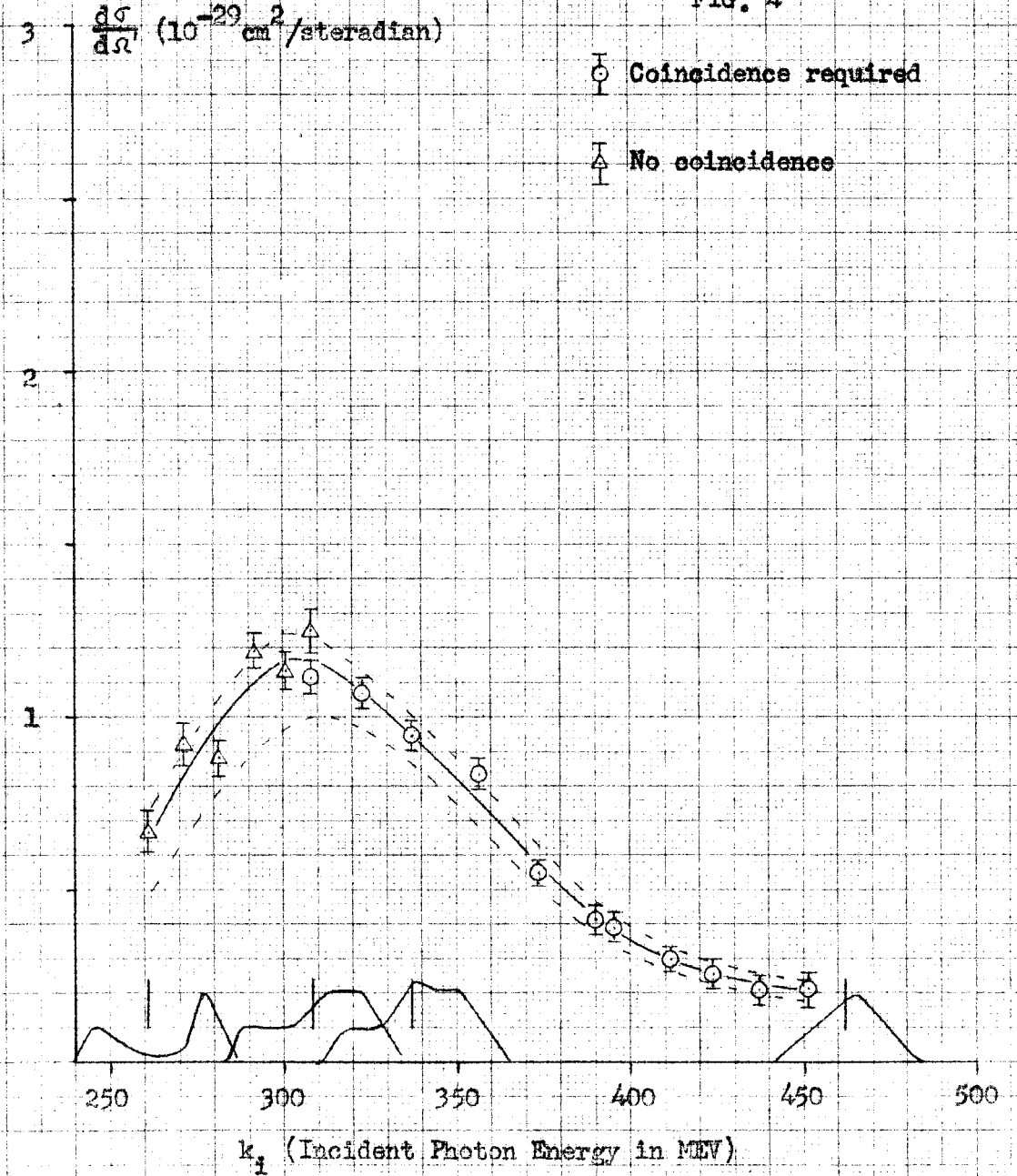

$$\gamma + P \rightarrow P + \pi^0$$

Center of mass differential cross section

for proton laboratory angle, θ_p = 19 1/2°

California Institute of Technology
July 31, 1954

FIG. 5

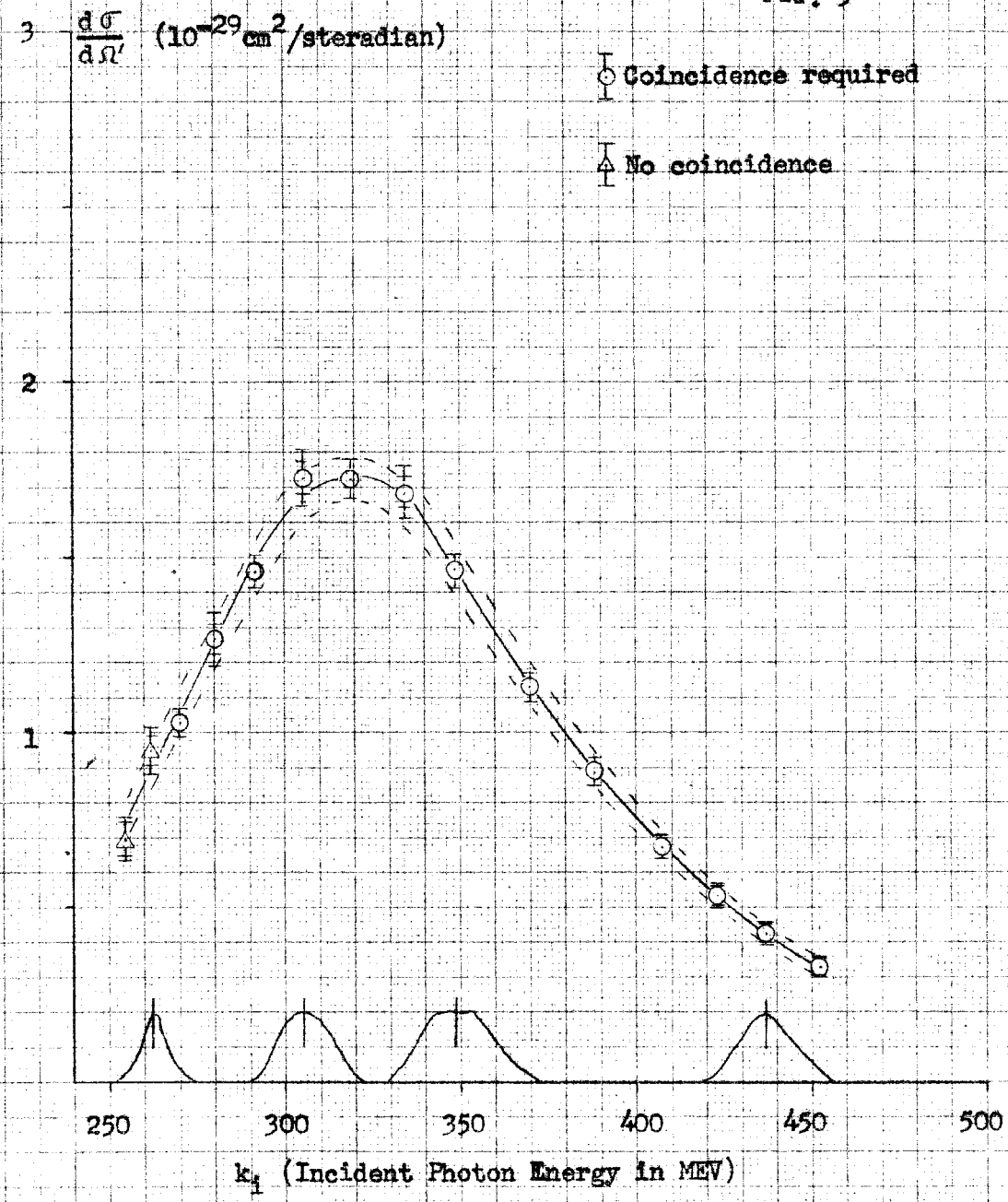

$$\gamma + p \longrightarrow p + \pi^{o}$$

Center of mass differential cross section

for proton laboratory angle, $\theta_p = 29^{o}$

California Institute of Technology
July 31, 1954

FIG. 6

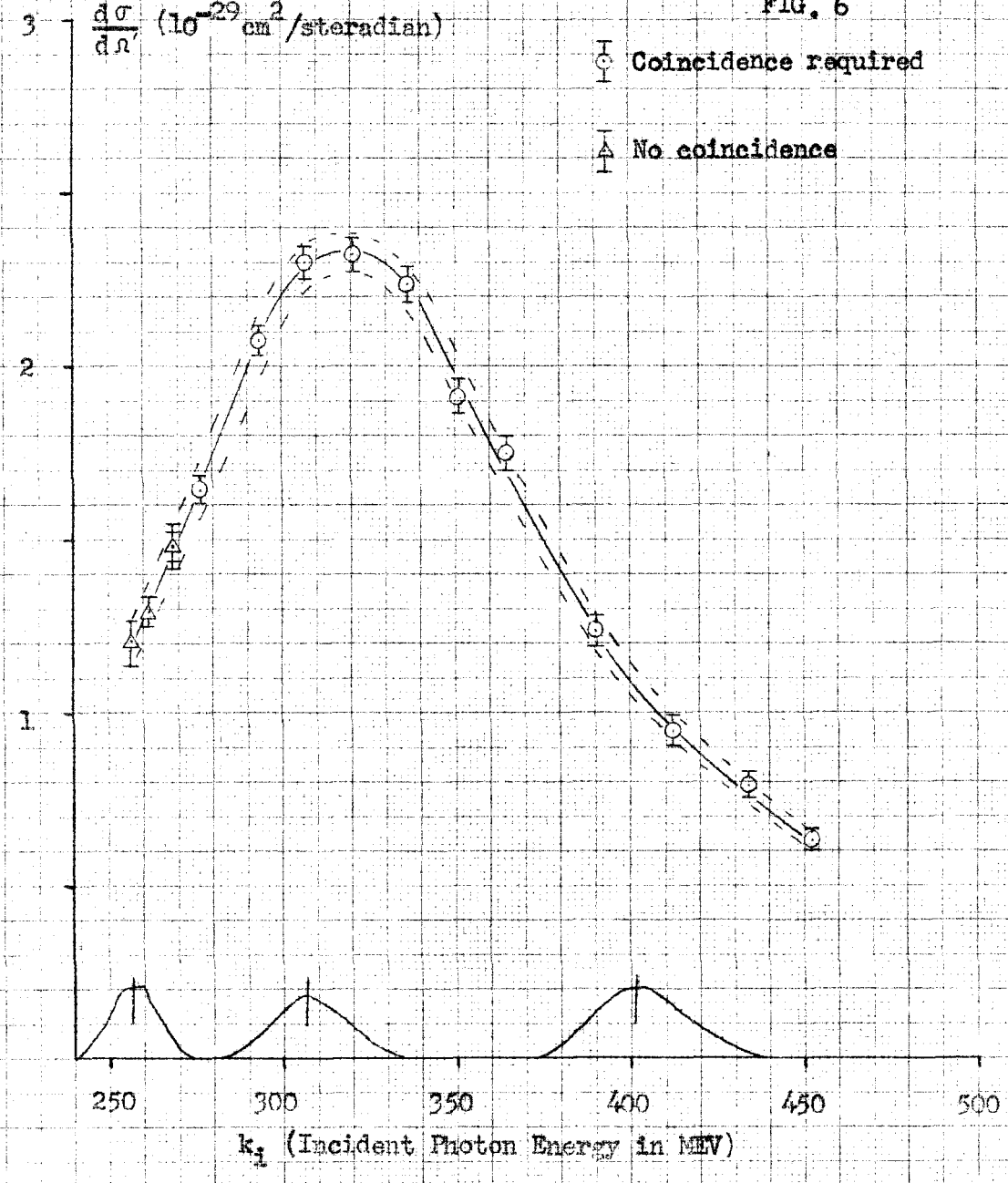

$$\gamma + P \rightarrow P + \pi^{o}$$

Center of mass differential cross section

for proton laboratory angle, θ_p = 40 1/2°

California Institute of Technology
July 31, 1954

FIG. 7

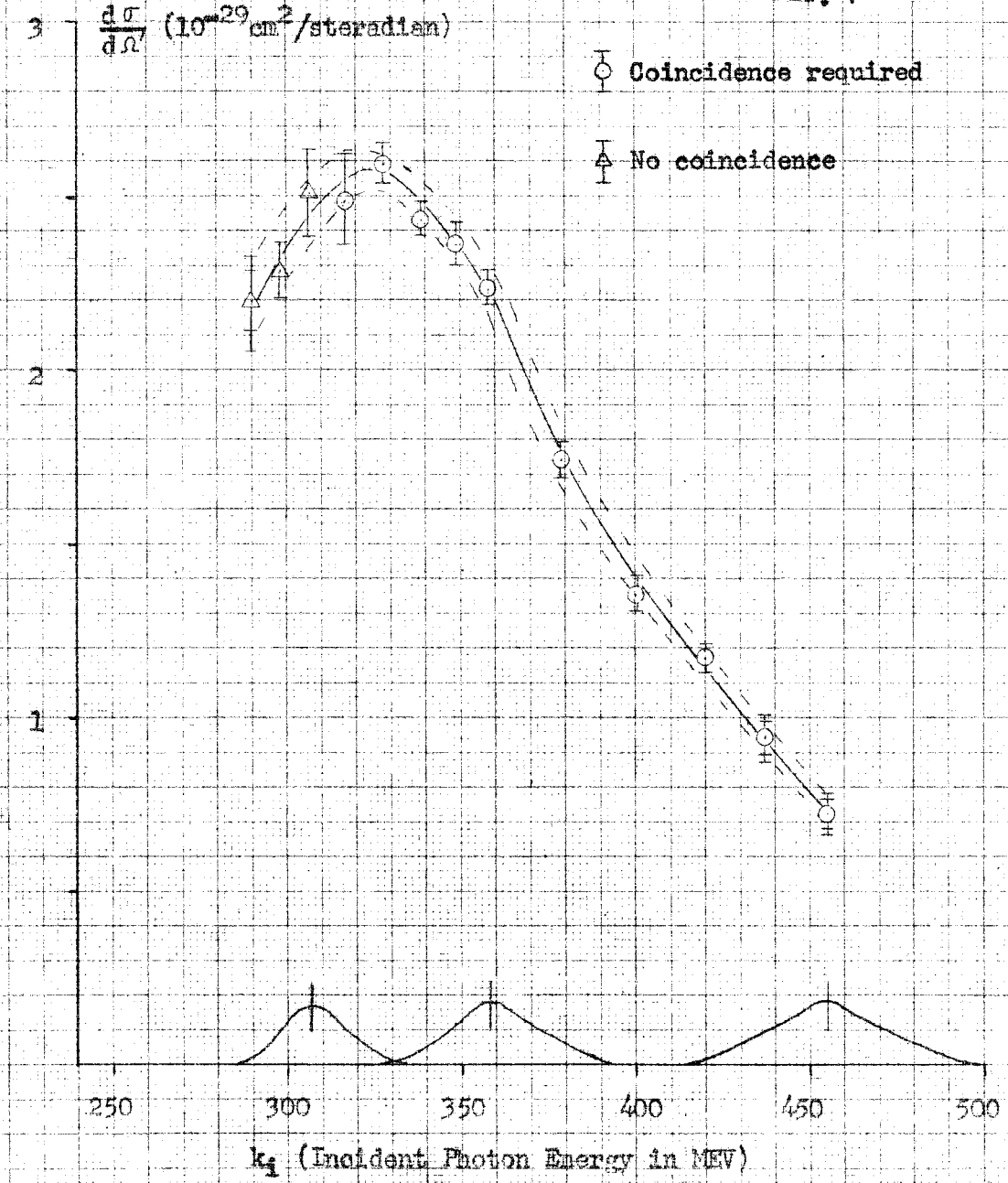

$$\gamma + {}^{47}P \rightarrow P + \pi^{0}$$

Center of mass differential cross section

for proton laboratory angle, θ_p = 50 1/4°

California Institute of Technology
July 31, 1954

FIG. 8

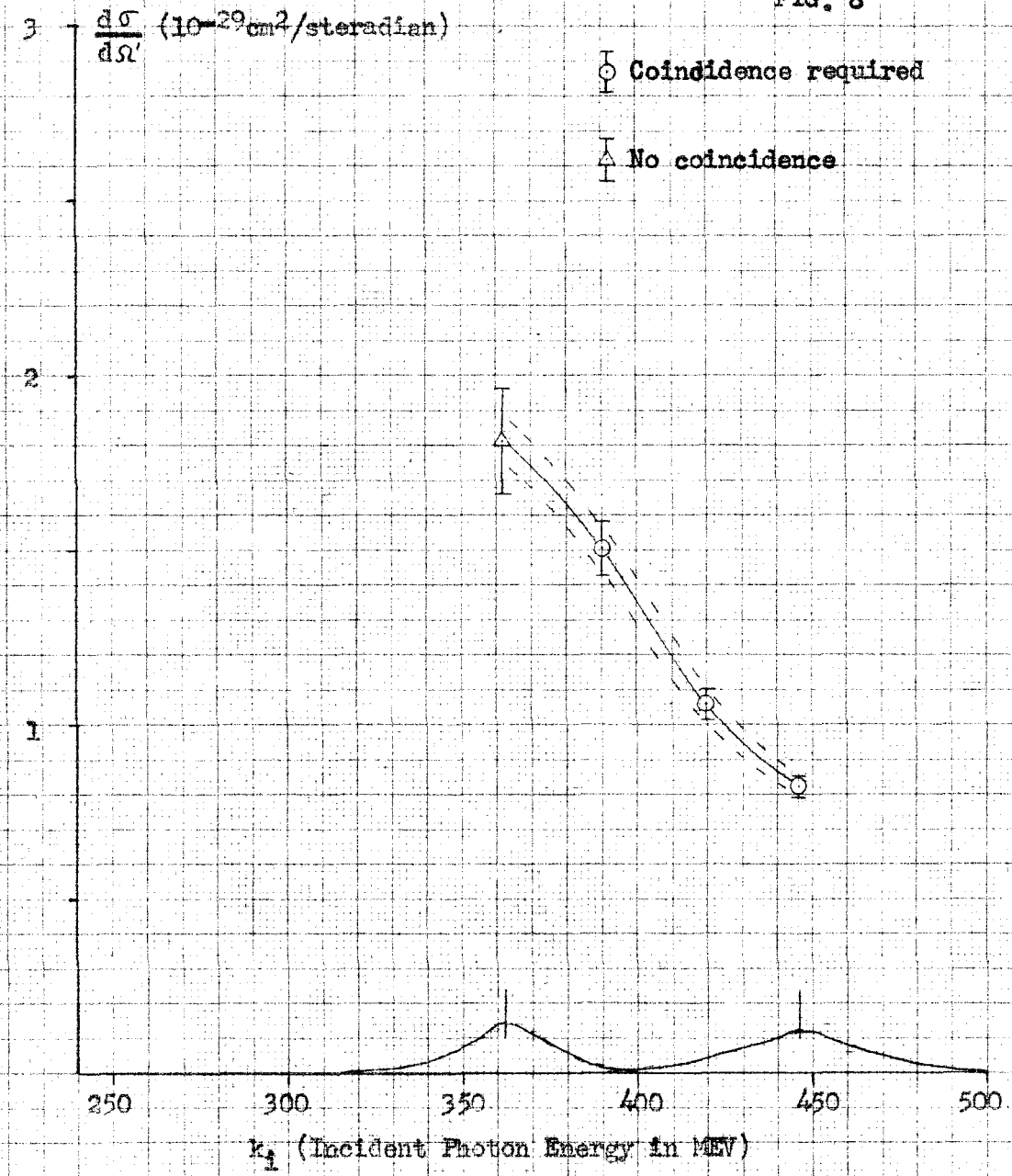

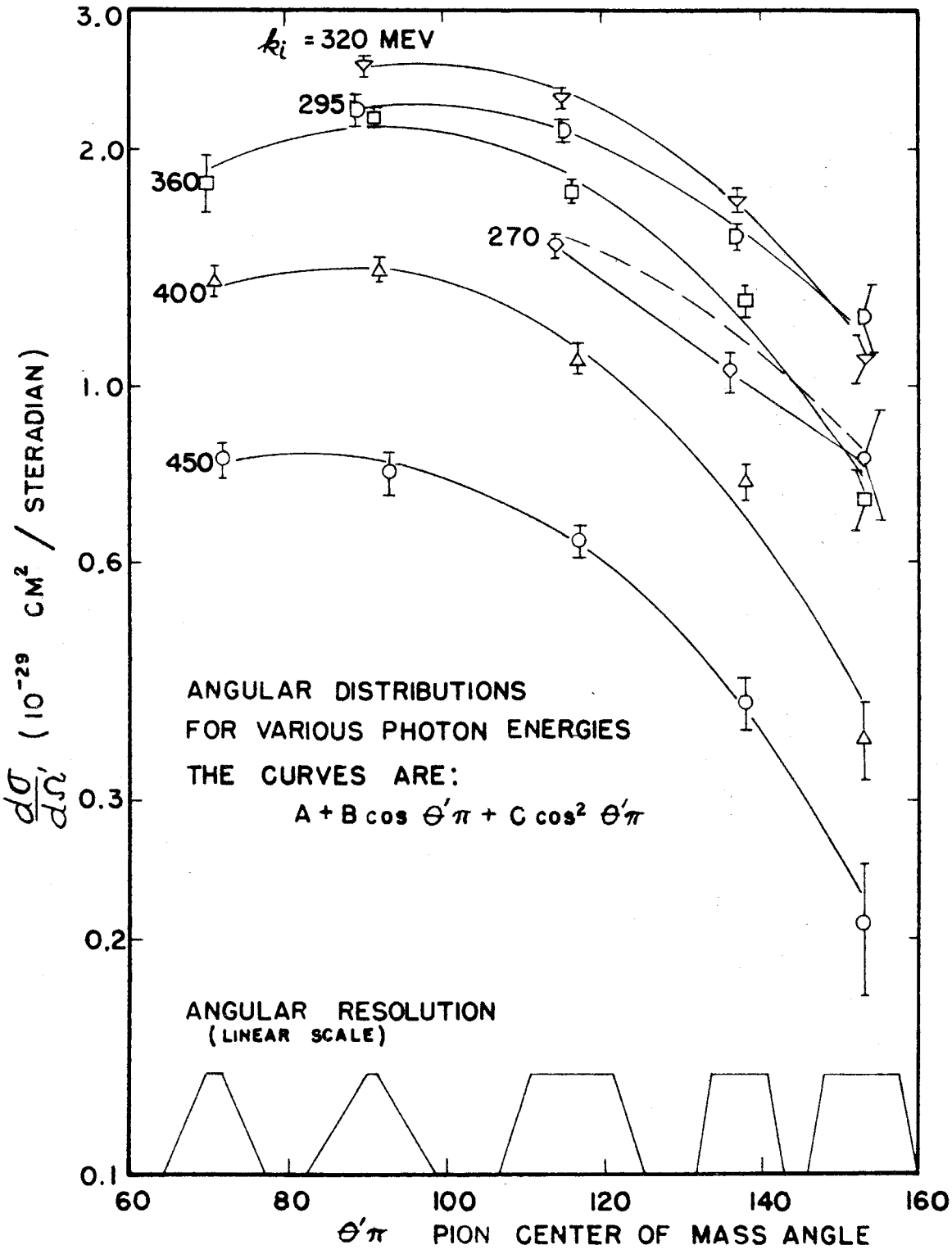
3.0
2.0
1.0
0.6
0.3
0.2
0.1
k_i = 320 MEV
295
360
270
400
450
ANGULAR DISTRIBUTIONS
FOR VARIOUS PHOTON ENERGIES
THE CURVES ARE:
A + B cos θ'π + C cos² θ'π
ANGULAR RESOLUTION
(LINEAR SCALE)
$\frac{d\sigma}{d\Omega'}$ (10^{-29} CM² / STERADIAN)
60
80
100
120
140
160
θ'π PION CENTER OF MASS ANGLE

FIG. 9

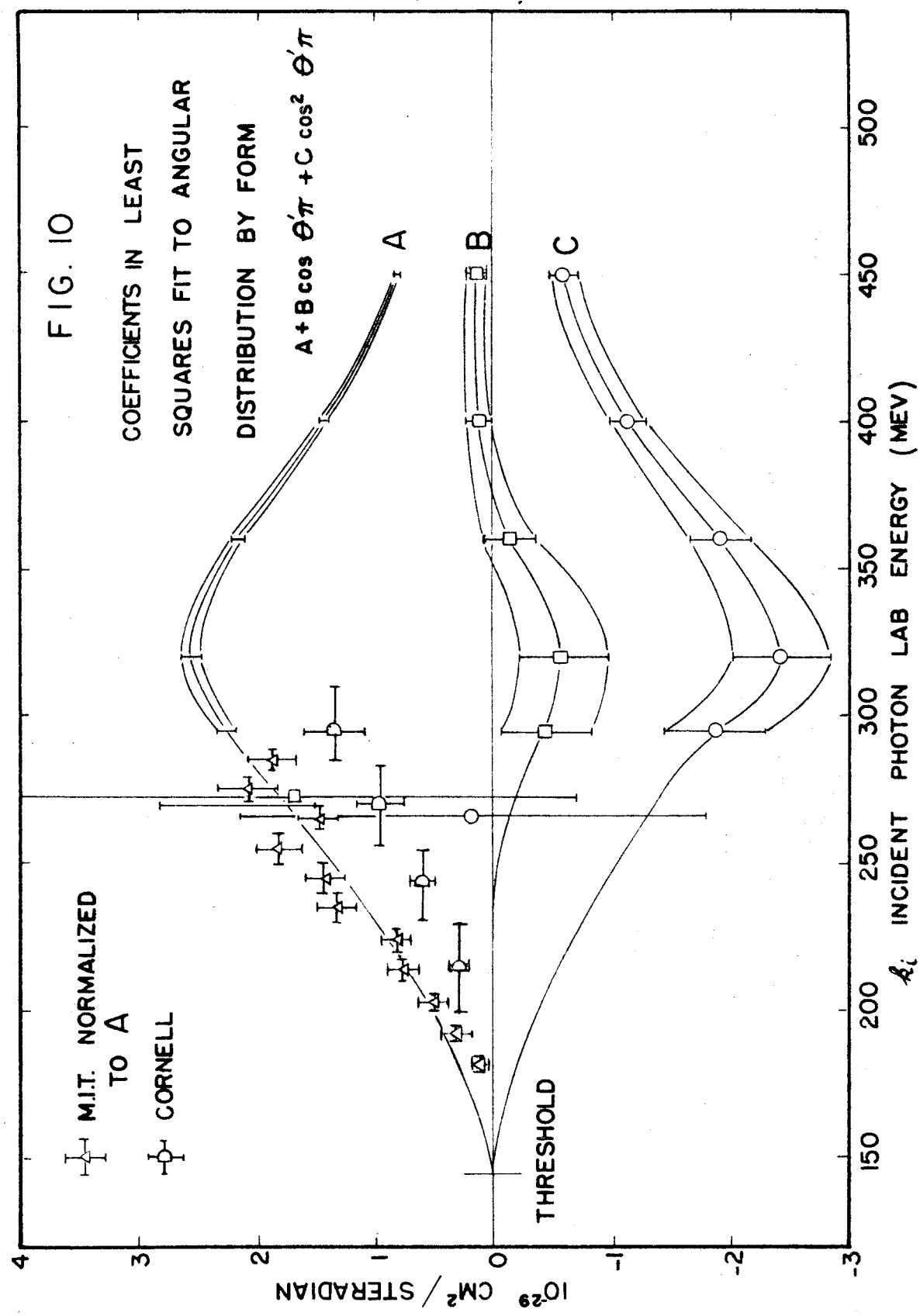
FIG. 10
COEFFICIENTS IN LEAST SQUARES FIT TO ANGULAR DISTRIBUTION BY FORM
A + B cos θ'π + C cos² θ'π
A
B
C
M.I.T. NORMALIZED TO A
CORNELL
THRESHOLD
10⁻²⁹ CM² / STERADIAN
4
3
2
1
0
-1
-2
-3
150
200
250
300
350
400
450
500
k_i INCIDENT PHOTON LAB ENERGY (MEV)

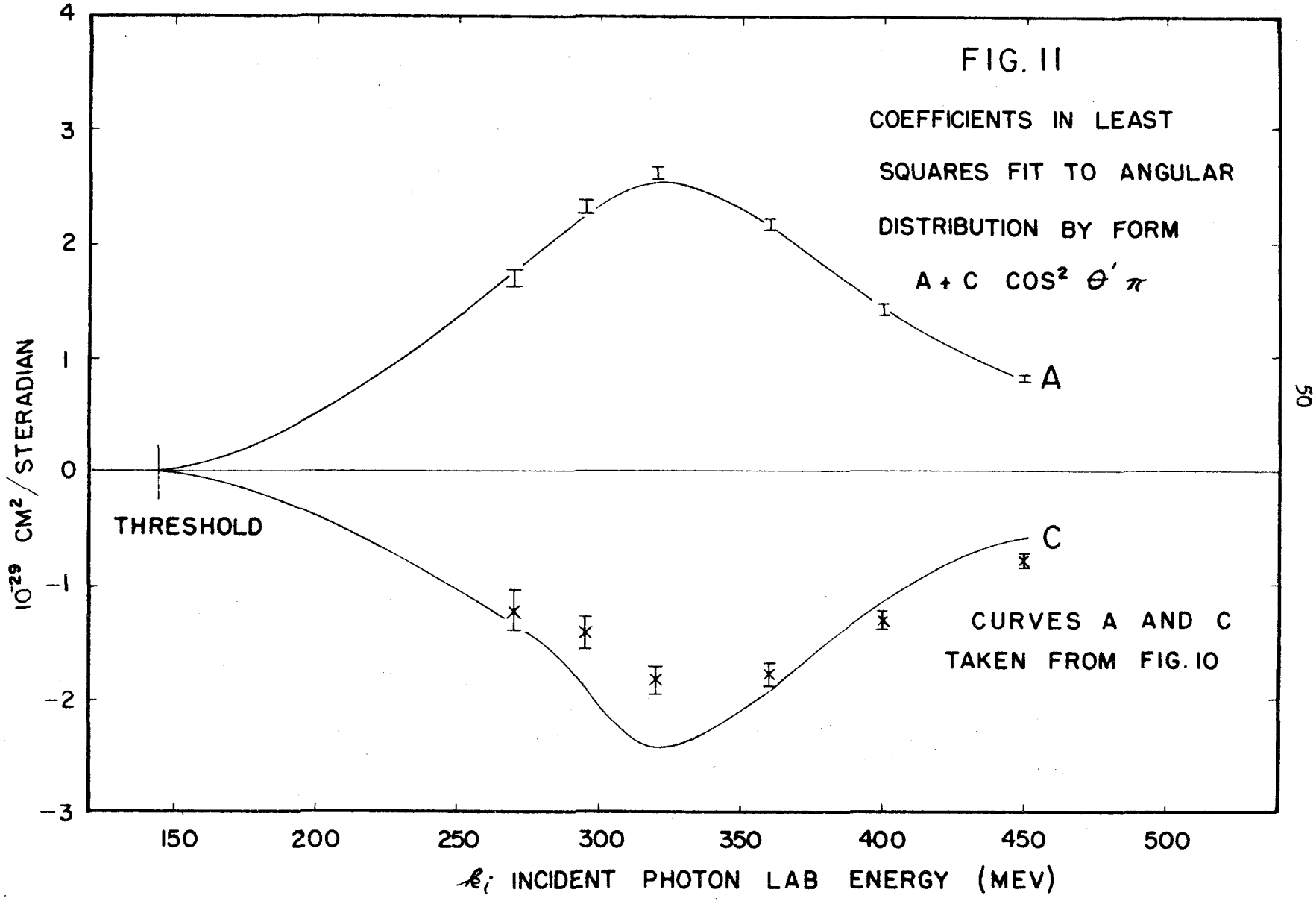
FIG. II
COEFFICIENTS IN LEAST SQUARES FIT TO ANGULAR DISTRIBUTION BY FORM
A + C COS² θ' π
A
C
THRESHOLD
CURVES A AND C TAKEN FROM FIG. 10
10⁻²⁹ CM²/STERADIAN
4
3
2
1
0
-1
-2
-3
150
200
250
300
350
400
450
500
k_i INCIDENT PHOTON LAB ENERGY (MEV)

$\sigma/(\lambda'_\gamma)^2$

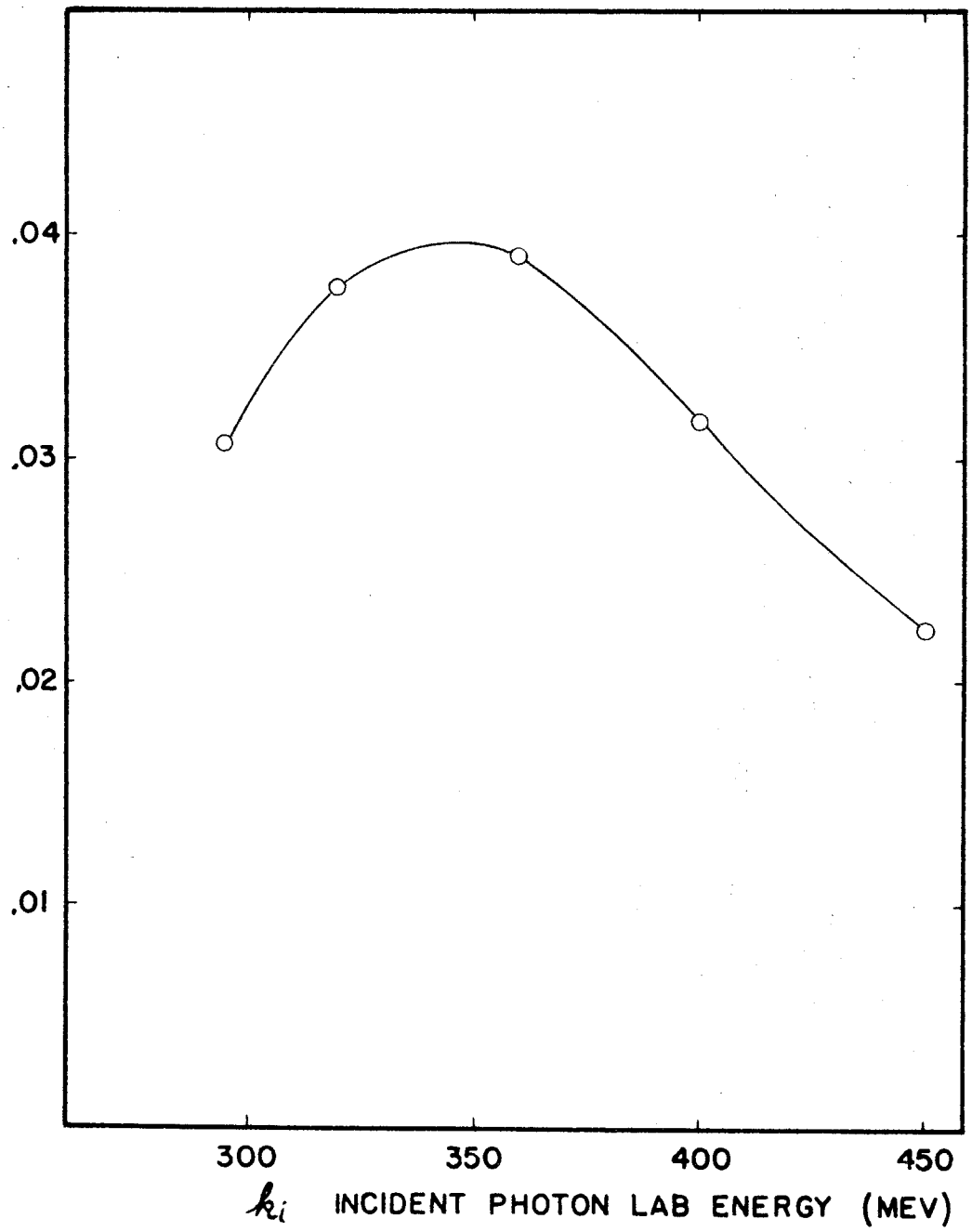

FIG. 12

FIG. 13

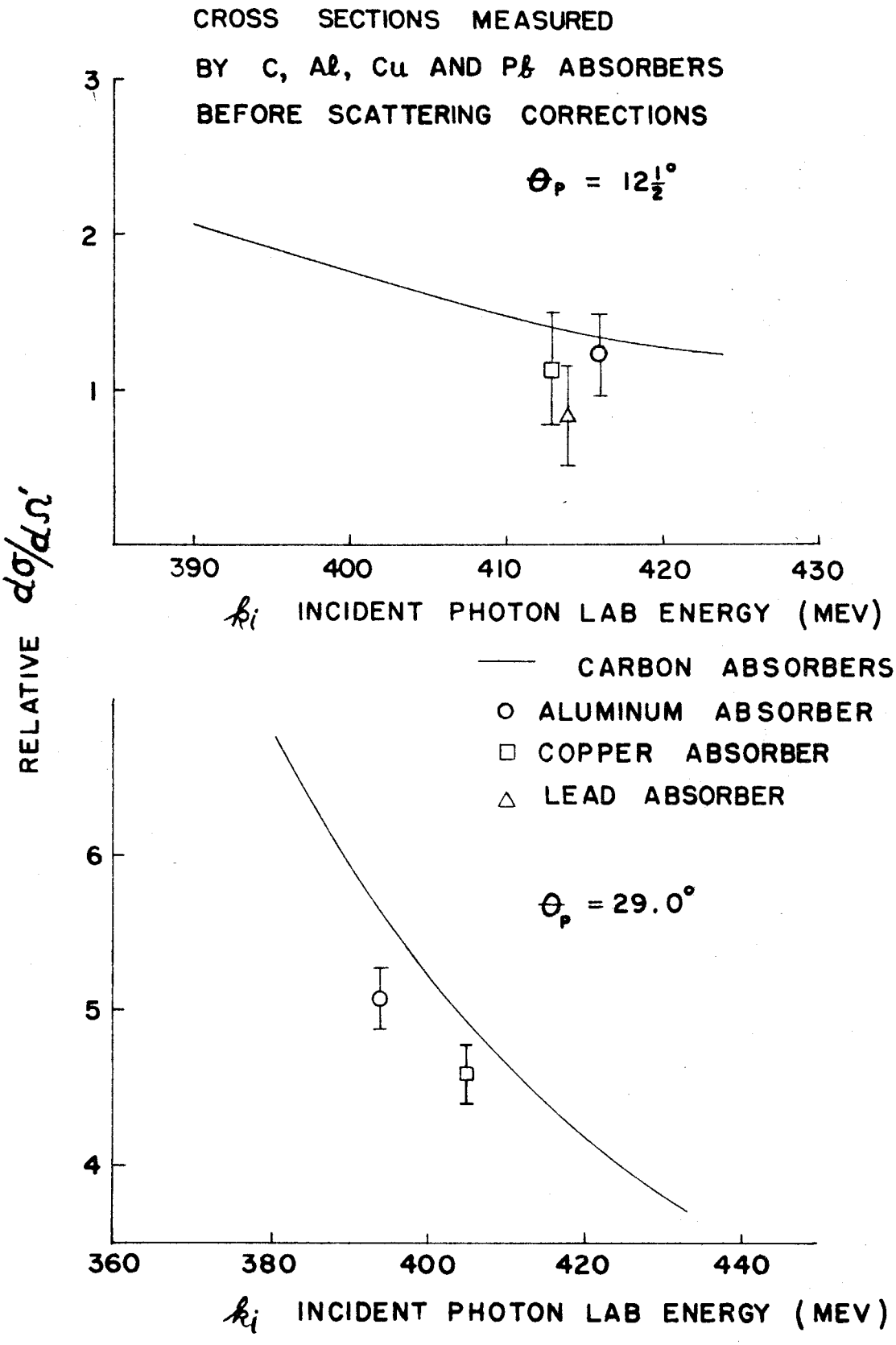
CROSS SECTIONS MEASURED
BY C, Al, Cu AND Pb ABSORBERS
BEFORE SCATTERING CORRECTIONS
$\theta_p = 12\frac{1}{2}^\circ$
3
2
1
390
400
410
420
430
k_i INCIDENT PHOTON LAB ENERGY (MEV)
RELATIVE $d\sigma/d\Omega'$
CARBON ABSORBERS
ALUMINUM ABSORBER
COPPER ABSORBER
LEAD ABSORBER
$\theta_p = 29.0^\circ$
6
5
4
360
380
400
420
440
k_i INCIDENT PHOTON LAB ENERGY (MEV)

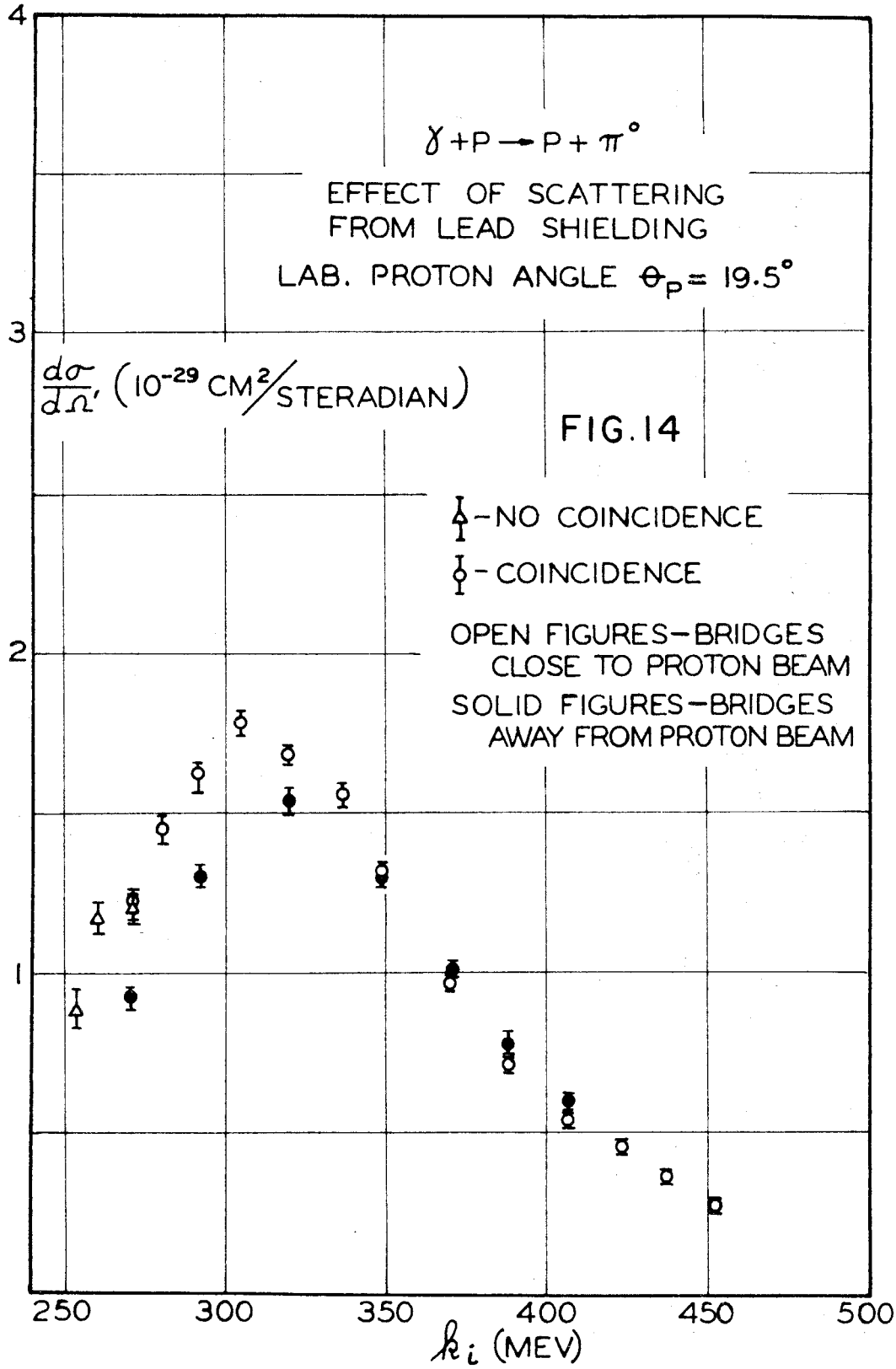
$\gamma + P \rightarrow P + \pi^\circ$
EFFECT OF SCATTERING
FROM LEAD SHIELDING
LAB. PROTON ANGLE $\theta_p = 19.5^\circ$
$\frac{d\sigma}{d\Omega}$ (10^{-29} CM^2/STERADIAN)
FIG. 14
-NO COINCIDENCE
-COINCIDENCE
OPEN FIGURES-BRIDGES CLOSE TO PROTON BEAM
SOLID FIGURES-BRIDGES AWAY FROM PROTON BEAM
4
3
2
1
250
300
350
400
450
500
k_i (MEV)

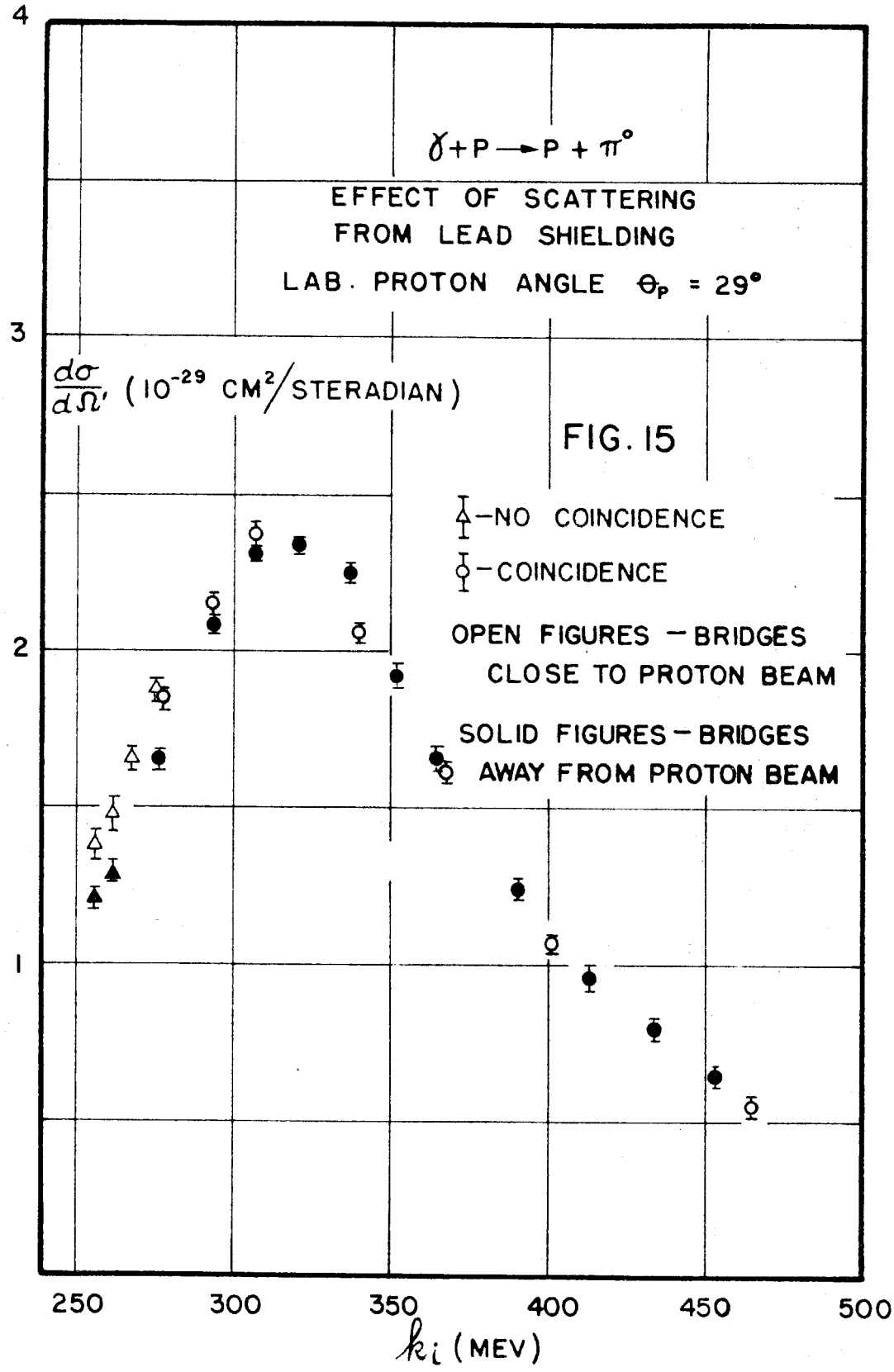
γ + P → P + π°
EFFECT OF SCATTERING
FROM LEAD SHIELDING
LAB. PROTON ANGLE θp = 29°
dσ/dΩ, (10⁻²⁹ CM²/STERADIAN)
FIG. 15
△—NO COINCIDENCE
○—COINCIDENCE
OPEN FIGURES — BRIDGES
CLOSE TO PROTON BEAM
SOLID FIGURES — BRIDGES
AWAY FROM PROTON BEAM
4
3
2
1
250
300
350
400
450
500
ki (MEV)

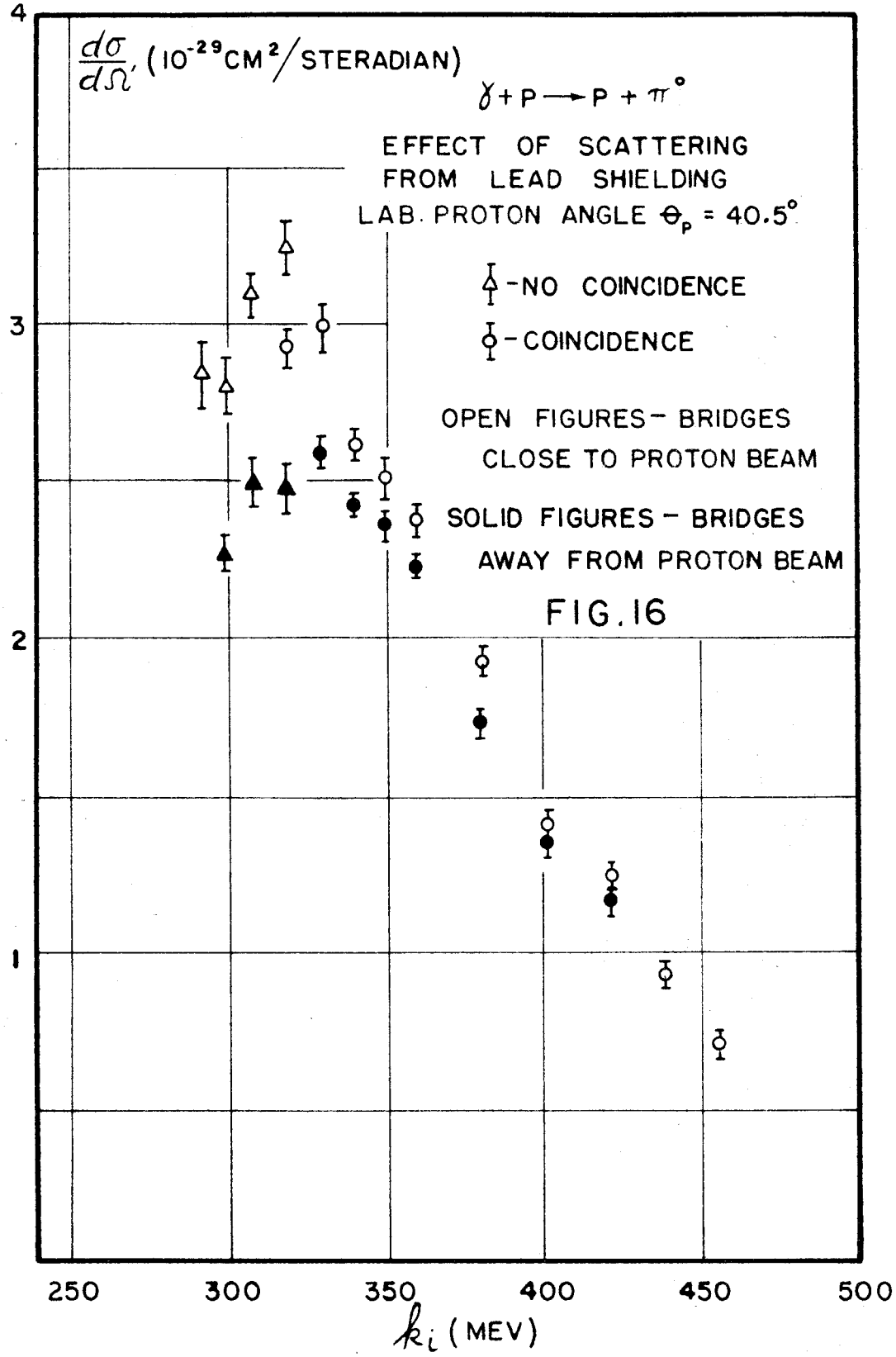
$\frac{d\sigma}{d\Omega}$, (10^{-29}CM^2/STERADIAN)
$\gamma + P \rightarrow P + \pi^\circ$
EFFECT OF SCATTERING
FROM LEAD SHIELDING
LAB. PROTON ANGLE $\theta_p = 40.5^\circ$
-NO COINCIDENCE
-COINCIDENCE
OPEN FIGURES- BRIDGES
CLOSE TO PROTON BEAM
SOLID FIGURES - BRIDGES
AWAY FROM PROTON BEAM
4
3
2
1
250
300
350
400
450
500
k_i (MEV)

FIG. 16

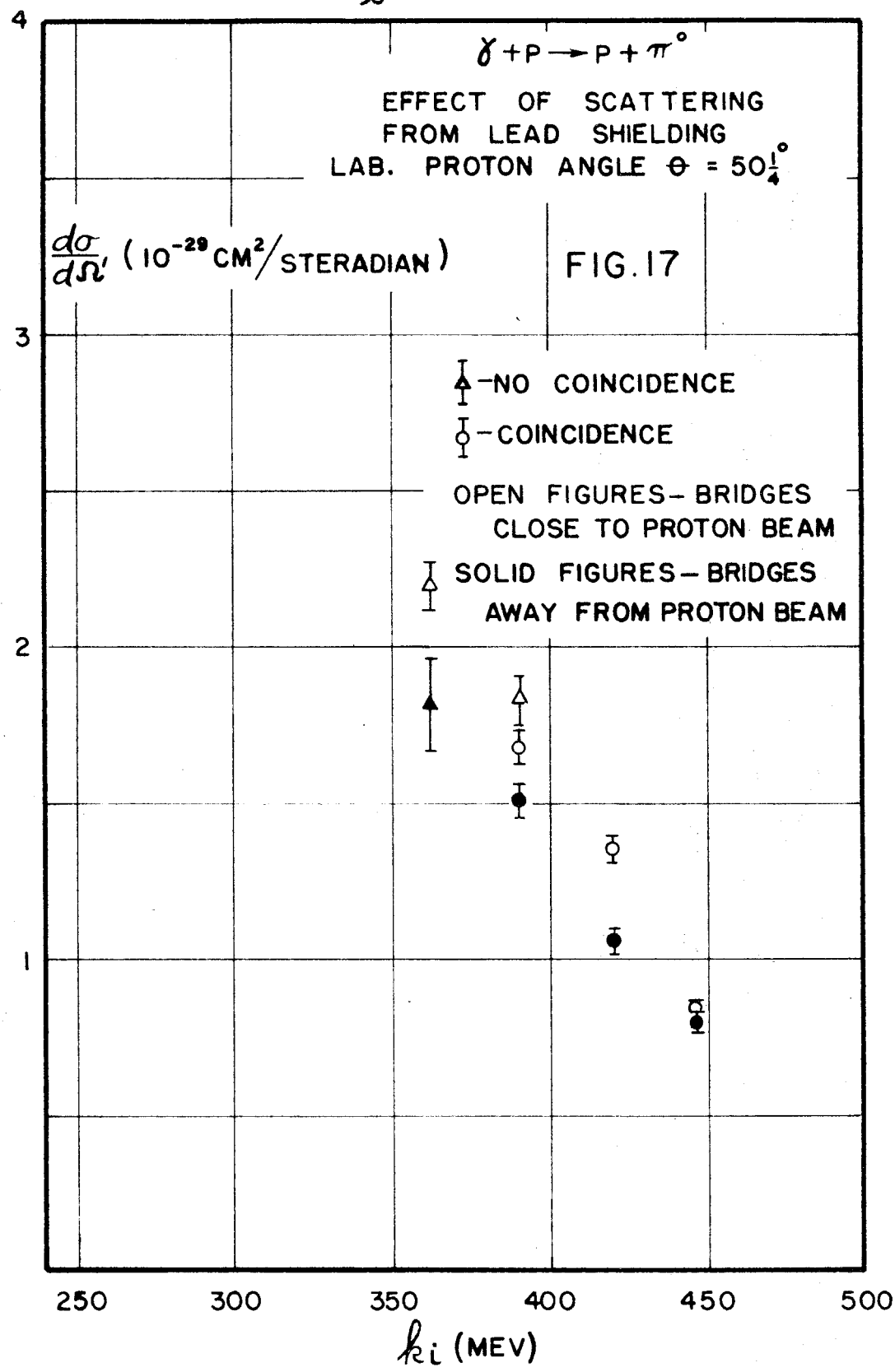
γ + P → P + π°
EFFECT OF SCATTERING
FROM LEAD SHIELDING
LAB. PROTON ANGLE θ = 50¼°
dσ/dΩ (10⁻²⁹ CM²/STERADIAN)
FIG. 17
-NO COINCIDENCE
-COINCIDENCE
OPEN FIGURES- BRIDGES
CLOSE TO PROTON BEAM
SOLID FIGURES- BRIDGES
AWAY FROM PROTON BEAM
4
3
2
1
250
300
350
400
450
500
kᵢ (MEV)

INVESTIGATION OF PROTON COMPTON EFFECT

CONCLUSION:

$\sigma(\gamma,P;P',\gamma')_{315\ MEV} \leq 0.025 \pm 0.025)\ \sigma(\gamma,P;P,\pi')_{355\ MEV}$

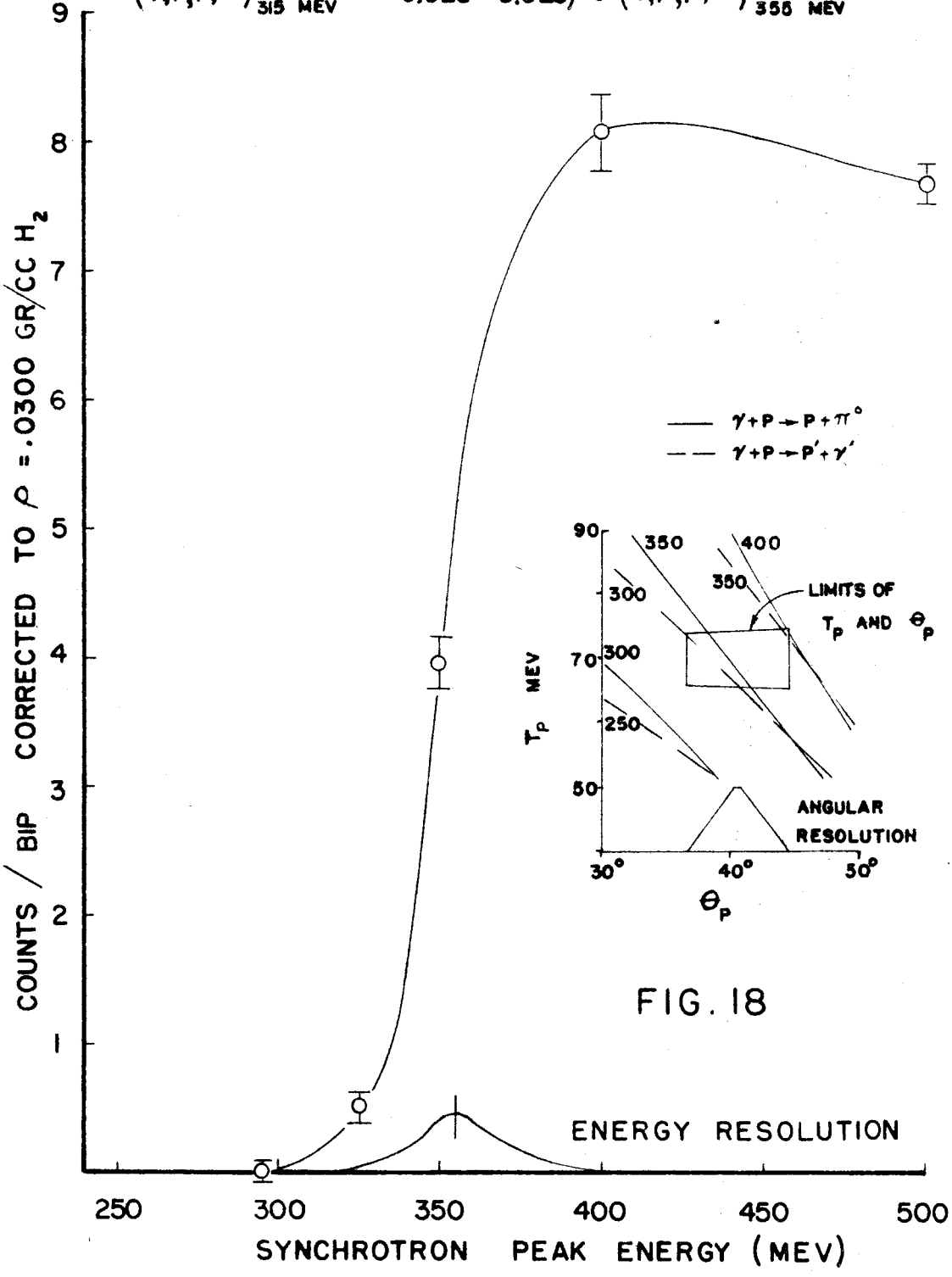

FIG. 18

CHECK OF $\gamma + P \rightarrow P' + \gamma'$ BY LOOKING AT $\gamma + P \rightarrow P + \pi^\circ$ ABOVE AVAILABLE γ ENERGY (500 MEV) ASSUMING $n(k_i) \propto \frac{1}{k_i}$

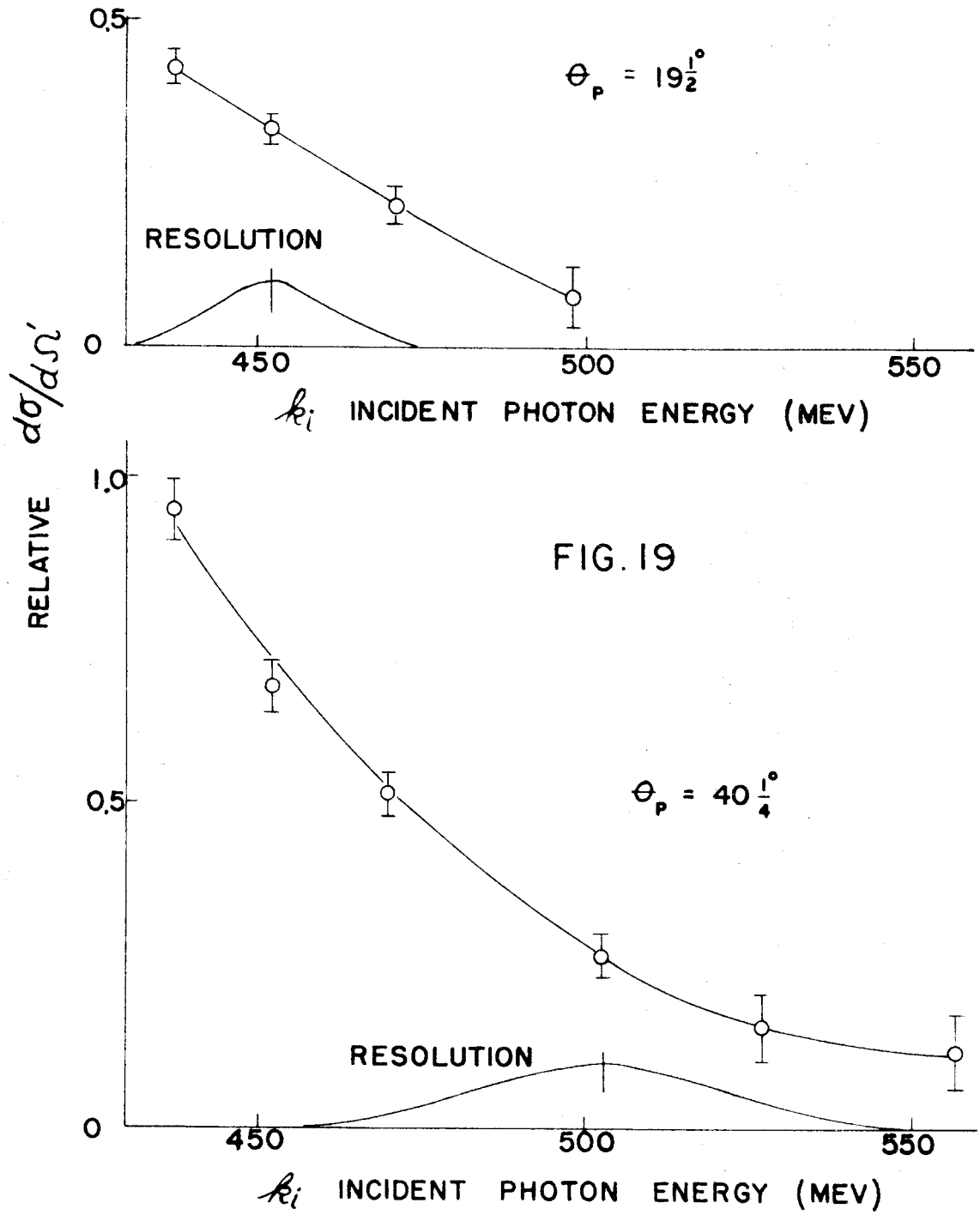

FIG. 19

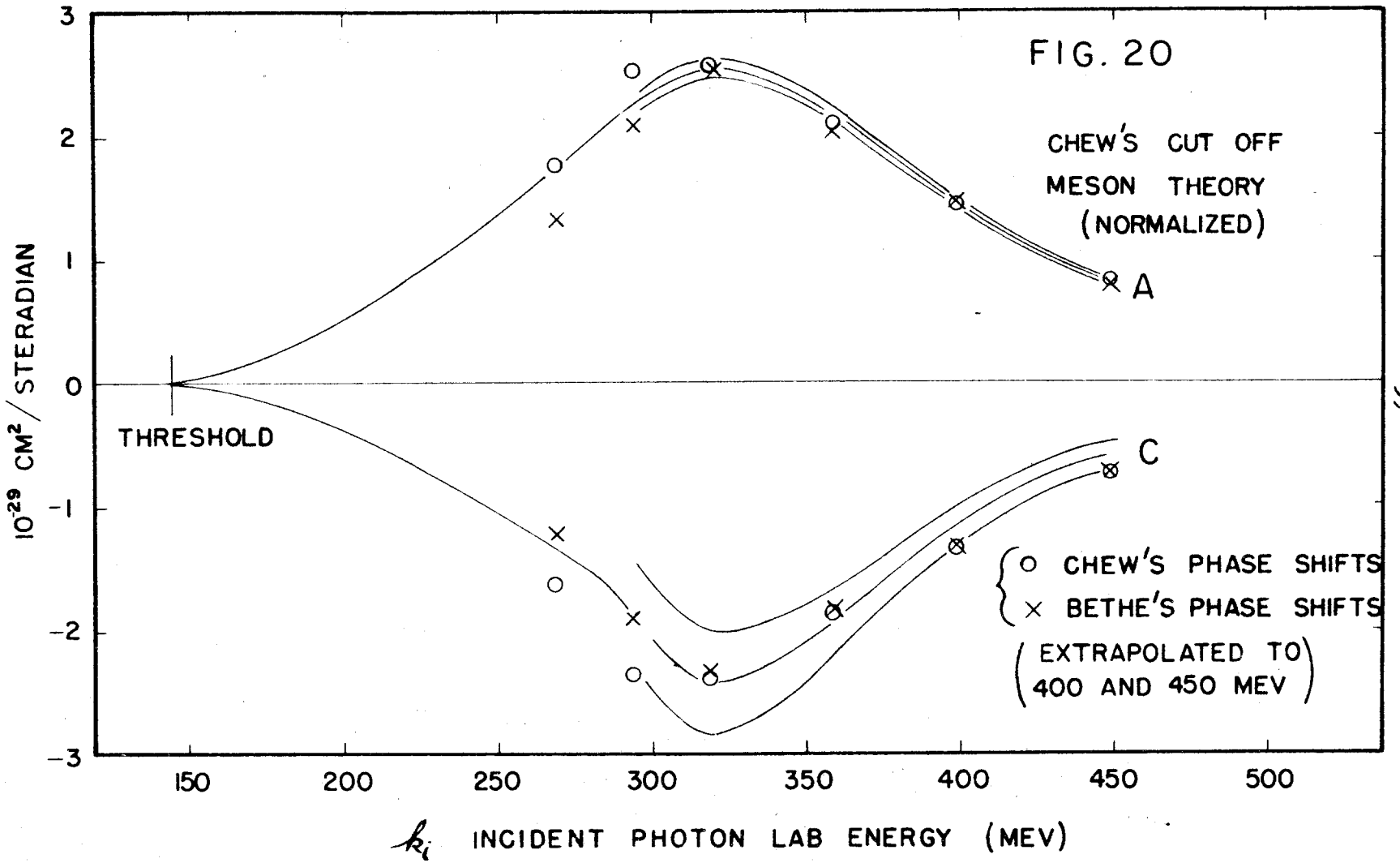
FIG. 20
CHEW'S CUT OFF
MESON THEORY
(NORMALIZED)
A
C
THRESHOLD
CHEW'S PHASE SHIFTS
BETHE'S PHASE SHIFTS
EXTRAPOLATED TO
400 AND 450 MEV
10^{-29} CM^2 / STERADIAN
3
2
1
0
-1
-2
-3
150
200
250
300
350
400
450
500
k_i INCIDENT PHOTON LAB ENERGY (MEV)

TABLE I

ANGULAR DISTRIBUTION OF $\gamma + P \longrightarrow P + \pi^{\circ}$

Lab. Angle		12 1/2°	19 1/2°	29°	40 1/2°	50 1/4°
Energy						
270	$\frac{d\sigma}{d\Omega'}$	.81±.13	1.05±.06	1.51±.05		
	θ_{π}'	153	136	114		
295	$\frac{d\sigma}{d\Omega'}$	1.23±.12	1.55±.06	2.12±.05	2.24±.09	
	θ_{π}'	153	137	115	89	
320	$\frac{d\sigma}{d\Omega'}$	1.09±.08	1.73±.06	2.33±.06	2.56±.08	
	θ_{π}'	153	137	115	90	
360	$\frac{d\sigma}{d\Omega'}$	.72±.06	1.29±.06	1.78±.06	2.20±.06	1.82±.15
	θ_{π}'	153	138	116	91	70
400	$\frac{d\sigma}{d\Omega'}$	.36±.04	.76±.04	1.09±.05	1.41±.05	1.36±.06
	θ_{π}'	153	138	117	92	71
450	$\frac{d\sigma}{d\Omega'}$	.21±.04	.40±.03	.64±.03	.78±.05	.81±.04
	θ_{π}'	153	138	117	93	72

$\frac{d\sigma}{d\Omega'}$ is in units of 10^{-29} cm^2/steradian

TABLE II

$j = 3/2$, $T = 3/2$ PHASE SHIFTS TO FIT A

T (MEV)	k_i (MEV)	δ_{33} (Chew)	δ_{33} (Bethe)	δ_{33} (Ross)
125	270	41	34	60
150	295	61	51	72
175	320	77	72	87
215	360	95	106	110
255	400	113	116	129
305	450	130	132	142

δ_{33}(Ross) and the last two of the other δ's were chosen to fit A